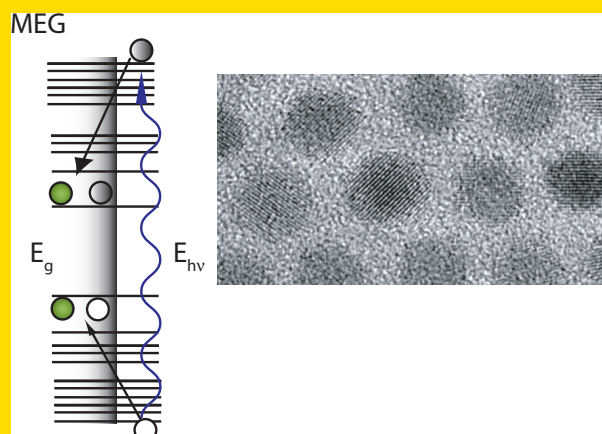


**Abstract** Within the range of photon energies illuminating the Earth's surface, absorption of a photon by a conventional photovoltaic semiconductor device results in the production of a single electron-hole pair; energy of a photon in excess of the semiconductor's bandgap is efficiently converted to heat through electron and hole interactions with the crystal lattice. Recently, colloidal semiconductor nanocrystals and nanocrystal films have been shown to exhibit efficient multiple electron-hole pair generation from a single photon with energy greater than twice the effective band gap. This multiple carrier pair process, referred to as multiple exciton generation (MEG), represents one route to reducing the thermal loss in semiconductor solar cells and may lead to the development of low cost, high efficiency solar energy devices. We review the current experimental and theoretical understanding of MEG, and provide views to the near-term future for both fundamental research and the development of working devices which exploit MEG.



Absorption of a single photon with energy in excess of two times the band gap,  $E_g$ , produces multiple excitons at the band edge. TEM picture of typical PbSe nanocrystals.

© 2008 by WILEY-VCH Verlag GmbH & Co. KGaA, Weinheim

## Multiple exciton generation in semiconductor nanocrystals: Toward efficient solar energy conversion

Matthew C. Beard\* and Randy J. Ellingson\*

National Renewable Energy Laboratory, Golden, CO 80401, USA

Received: 27 March 2008, Revised: 13 May 2008, Accepted: 26 May 2008

Published online: 16 July 2008

PACS: 78.47.jk, 78.67.Bf, 82.53.Mj

### 1. Introduction

Conventional single-junction photovoltaic (PV) devices such as those based on crystalline silicon routinely attain a relatively high efficiency of  $\sim 22\%$ , albeit with significant manufacturing costs associated with starting material purification, high-temperature processing steps, and strict parameter control. At present, the record laboratory efficiency for a crystalline Si (*c*-Si) solar cell stands at 24.7% under standard AM1.5G illumination [1]. The same type of solar cell reaches slightly higher conversion efficiency when used in a concentrator design (27.6% record efficiency) [2]. A thermodynamically ideal Si solar cell operating under conventional assumptions of one electron-hole pair per absorbed photon would convert about 33% of the incident AM1.5G sunlight to electrical power (Shockley-

Queisser limit) [3], and  $\sim 47\%$  of the incident power would turn into heat within the cell. The majority of losses result when a photon is absorbed with energy greater than the bandgap of Si and the resultant carrier undergoes fast cooling via phonon scattering and emission (Fig. 1a). Therefore, surpassing the Shockley-Queisser limit requires an expansion of the PV device complexity to efficiently convert a wider range of the solar spectrum. The primary example involves the use of multiple absorber materials with varying bandgaps (largest bandgap as the top absorber); such a device more efficiently converts a wide range of photon energies and effectively reduces conversion efficiency losses to thermal energy. Specifically, the use of triple-junction device designs has enabled an integrated solar cell based on GaInP, GaInAs, and Ge to attain an efficiency of 40.7% for concentrated sunlight [4]. However, the III-V multi-

\* Corresponding authors: e-mail: matt.beard@nrel.gov, randy.ellingson@nrel.gov

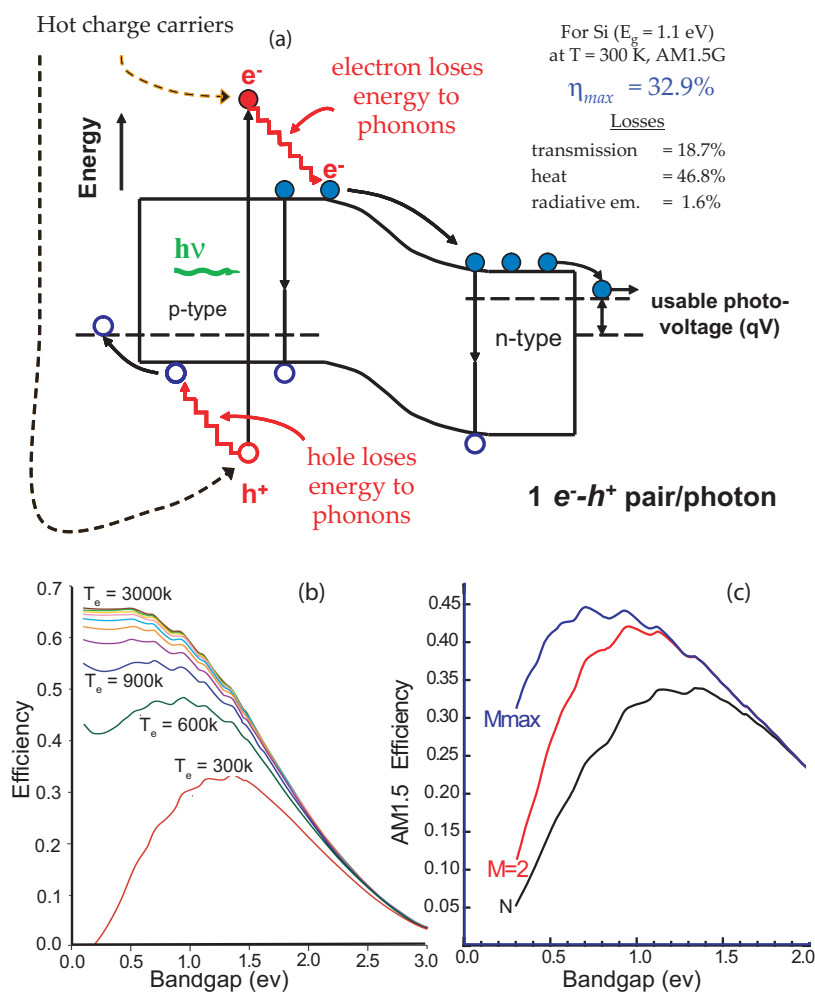


**Figure 1** (online color at: [www.lpr-journal.org](http://www.lpr-journal.org)) (a) Schematic of a traditional  $p-n$  junction solar cell. Light that is absorbed with photon energies greater than the bandgap produces carriers (electron and holes) with excess kinetic energy. These 'hot' carriers lose energy by scattering and emitting phonons with the lattice. Heat loss makes up  $\sim 47\%$  of the energy conversion losses. (b) If the carriers could be extracted with no heat loss the thermodynamically allowed conversion efficiency could be doubled to  $\sim 67\%$  [8],  $T_e$  is the hot carrier temperature. (c) Enhancement expected from an increased photocurrent due to carrier multiplication [9],  $N$  is the Shockley-Queisser limit,  $M=2$  is for extracting 2 carriers per absorbed photon at  $E_{hv} > 2E_g$ , and  $M_{max}$  is extracting  $M$  carriers at  $E_{hv} > ME_g$ . In (b) the photo-voltage is increased while in (c) the photo-current is enhanced.

junction concentrator cells carry a very high manufacturing cost due to the high number of layers (each requiring a separate growth step) and the vacuum requirements for high quality epitaxial crystal growth.

An ideal technology would circumvent heat losses in a relatively simple device design, such as a single junction solar cell. Such a device would utilize the excess energy of hot-carriers (Fig. 1b) either by extracting them prior to thermalization (hot-carrier solar cells) [5] yielding a higher photo-voltage, or by generating multiple electron-hole pairs per photon via a carrier multiplication process to enhance the photocurrent [6, 7]. If carriers can be extracted without heat losses, the thermodynamically allowed efficiency would approximately double to  $\sim 67\%$  under standard AM1.5G illumination (Fig. 1b) [8]. Under concentrated sunlight, this value can even be higher. A carrier multiplication process where an electron with sufficiently high kinetic energy can generate one or more additional electron-hole pairs through a scattering process known as impact ionization would increase the theoretically attainable efficiency by  $\sim 30\%$  from 33 to 43% (Fig. 1c) [9]. Impact ionization does not occur in conventional PV devices with a rate sufficiently high to enhance device efficiency

within the solar spectrum. However, substantial gains would result from a PV device for which each absorbed photon of sufficient energy efficiently generates multiple electron-hole pairs which also contribute efficiently to the collected photocurrent (Fig. 1c).

The unique optical properties of quantum-confined semiconductor nanocrystals (NCs), including atomic-like electronic structure and size-dependent bandgap energies, make them interesting materials for potential application in optoelectronic devices such as solar cells. Large intra-band energy gaps equivalent to several optical phonon quanta open up at small NC sizes, suggesting the possibility that carrier cooling rates may slow due to the decreased efficiency of simultaneous multi-phonon scattering events (an effect referred to as the phonon bottleneck) [5]. Slowed cooling would enable interfacial charge transfer and/or impact ionization processes (carrier multiplication rates) to compete with the rate of carrier relaxation, potentially improving the performance of photoconversion devices. In addition, spatial confinement results in strong carrier-carrier interactions within NCs (an electron-hole pair confined to a NC is typically referred to as an exciton). Observations of photoluminescence (PL) blinking observed in single-NC

measurements [10] were ascribed to the process of Auger ionization [10, 11] in which exciton-exciton annihilation (Auger recombination) ejects an electron out of the NC core, resulting in a charged nanocrystal for which emission is quenched. The strong Coulomb interactions correlate with the prominent role played by Auger recombination within NCs occupied by more than one exciton. The PL blinking effect, together with the prospect of a phonon bottleneck to slow carrier cooling, led Nozik to propose that the inverse of Auger recombination, impact ionization, may occur with higher efficiency in semiconductor NCs [5, 12].

Subsequent to Nozik's prediction of enhanced impact ionization in quantum-confined semiconductor NCs, experimental measurements on colloidal solutions of PbSe, PbS, and PbTe NCs revealed evidence of the single-photon generation of multiple excitons following pulsed excitation at high photon energy and low intensity, as evidenced by the signature of Auger recombination within the exciton population decay traces [13–15]. These measurements represented the first observations of multiple exciton generation in NCs. Analysis of the data indicated that single photon generation of multiple excitons occurs on a very short time scale following photon absorption, with an efficiency that increases with the energy of the photon. Because of the very high observed efficiency of multiple exciton production, the process has been referred to as multiple exciton generation (MEG), or carrier multiplication, to differentiate it from the impact ionization (I.I.) occurring in bulk semiconductors. Subsequent measurements led to the report of as many as seven excitons per photon for large PbSe NCs photoexcited at  $h\nu = 7.8E_g$  for  $E_g = 0.636$  eV [16]. A common misperception holds that the MEG process is intensity-dependent and relies on nonlinearities induced by the high peak power attained within short laser pulses used for excitation. To date, all published data support the conclusion of linearity with intensity for the MEG effect, though the ultimate remaining measure is to show conclusively that MEG occurs efficiently under steady-state one-sun levels of illumination – i.e., within an operating solar cell.

If achieved, optimized MEG-active NC-based solar energy conversion would enable a relatively simple single-junction device to capture a wide range of the solar spectrum, and simultaneously make efficient use of the higher energy photons through the generation of multiple excitons for photon energies exceeding  $2E_g$ . Modeling conducted under the assumptions of detailed balance, no nonradiative recombination losses, AM1.5G simulated solar illumination, and operation at the thermodynamic limit, concludes that a device converting all photons of  $h\nu > 2E_g$  to two electron-hole pairs would perform with 42% efficiency [9], far exceeding the 33% one-sun efficiency calculated by Shockley and Queisser in 1961 with identical assumptions but without any carrier multiplication processes in effect [3]. The potentially less-costly synthesis and fabrication of NC starting materials and solar cells warrants MEG-active NC-based solar cells as one promising avenue toward inexpensive and efficient solar energy.

Recently, MEG in semiconductor NCs has received considerable attention and has brought a renewed interest in understanding and measuring the dynamics of photo-generated carriers in semiconductor NCs. We review the current status of MEG and related carrier dynamics in the context of solar energy conversion. The outline of our presentation is as follows: In Sect. 1.1 we provide a brief introduction to semiconductor NC photophysics as background for the remaining article; for more detailed reviews we refer readers to the many books and review articles on this topic [17–19]. Sect. 1.2 introduces readers to femtosecond transient absorption measurements in semiconductor NCs. Sect. 2.1 provides background information on charge carrier dynamics in bulk semiconductor crystals. Sect. 2.2 addresses carrier cooling in semiconductor NCs. Sect. 2.3 introduces photon absorption statistics and multiexciton recombination characteristics of NCs. Sects. 2.4 and 2.5 cover MEG in NC samples: measurement, analysis, and other aspects. Sect. 3 reviews specific MEG research results for the various semiconductor NC types which have been studied, addressing the threshold photon energy as well as the reported QY values. Sect. 4 reviews current theoretical models used to describe the MEG mechanism. Sect. 5 discusses current activity in using NCs as the active layer within device designs enabling efficiencies enhanced by MEG. Sect. 6 discusses future directions.

### 1.1. Introduction to semiconductor NCs

Semiconductor NCs have sustained tremendous interest in the chemistry and physics communities because of dramatic size-dependent effects [18]. Reducing the physical dimensions of the NCs near to and below the Bohr exciton radius, quantization and interface effects become important and as a result many intrinsic material properties become size- and surface-dependent. Extensive theoretical and experimental study of semiconductor nanostructures over the past quarter century has dramatically broadened our understanding of fundamental issues such as size-dependent electronic structure [20–22], charge carrier relaxation dynamics and mechanisms [23–27], the influence of surfaces, interfaces, and barriers on recombination pathways [28, 29], and the nature and effects of Auger recombination [30]. In the case of colloidal semiconductor NCs (Fig. 2a), spatial confinement for NC diameters below the Bohr exciton radius results in significant blue-shifting of the absorption bandedge (effective bandgap). Fig. 2b displays the absorption onset for a series of PbSe NCs samples with average diameter ranging from 3.3 nm to 8.1 nm. As one example, 4.8 nm diameter PbSe NCs show an effective bandgap of  $\sim 0.82$  eV, exhibiting a strong confinement-induced blue shift of  $> 500$  meV compared to the bulk PbSe bandgap of  $\sim 0.28$  eV (the Bohr exciton radius in PbSe is 46 nm) [31]. The as-produced NCs are nearly spherical single crystals suspended in solution, and the NCs rarely show twinning or other core defects. Due to the very high ratio of surface area to volume, scaling as  $3/r$  for spherical particles, NC surface chemistry plays a

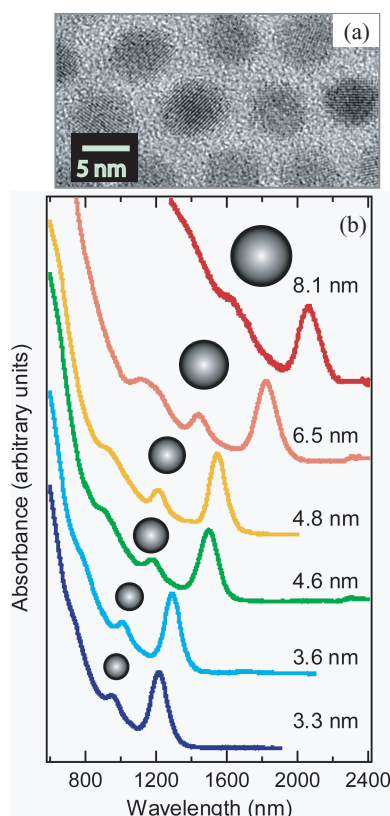


**Figure 2** (online color at: [www.lpr-journal.org](http://www.lpr-journal.org)) (a) TEM image showing PbSe NCs with average diameter of 5.2 nm. (b) Linear absorption spectra of a series of PbSe NCs with average diameter ranging from 3.3 nm to 8.1 nm. Strong excitonic absorption and a blue-shift of the onset are signatures of quantum confinement in NCs.

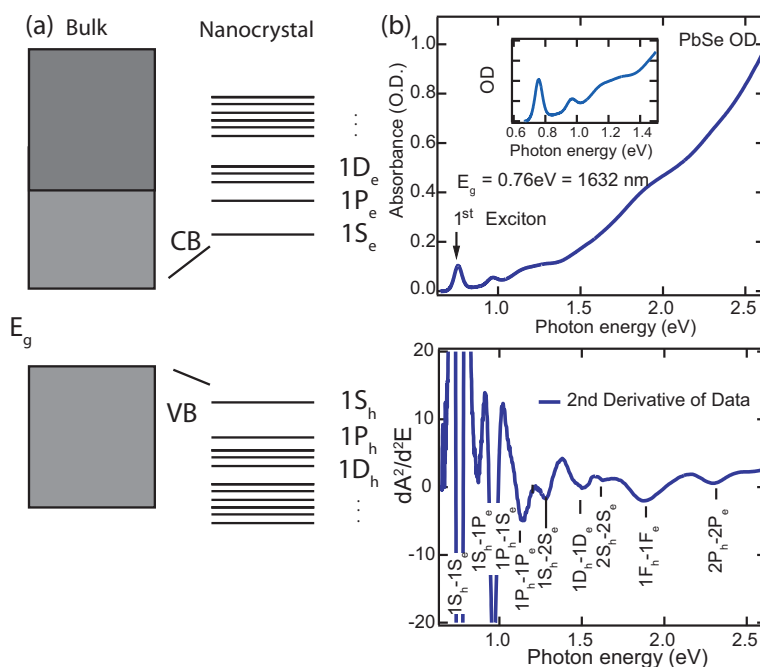


**Figure 3** (online color at: [www.lpr-journal.org](http://www.lpr-journal.org)) (a) In bulk semiconductors the valence (VB) and conduction (CB) bands form a continuum of electronic states with a gap, and the Fermi energy lies within the gap. In NCs the quantum confinement produces discrete states in the conduction and valence bands. (b) Transitions between these states can be seen in the absorption spectrum and assigned according to a  $k \cdot p$  analysis [14, 32] where envelope functions are used to describe the excitonic states.

very important role in charge carrier relaxation and recombination. In addition, semiconductor nanostructures present a unique system for the study of charge carrier dynamics within quantum confined materials.

Colloidal NCs serve as a zero-dimension material system owing to the presence of large potential barriers consisting of, for example, organic surface-capping molecules together with nonpolar solvents such as toluene, hexane, and tetrachloroethylene. HOMO-LUMO energy separations for the barrier agents are typically  $> 4$  eV, confining both electron and hole. An electron and hole confined within a NC of diameter near to or less than the Bohr exciton size interact strongly with one another through Coulomb forces, and are referred to here as an exciton. As the size of a semiconductor nanocrystal decreases below the bulk semiconductor's Bohr exciton size, the exciton experiences increasingly strong confinement effects which significantly alter the allowed energy levels and result in a size-dependent and increasingly discrete electronic structure (Fig. 3a). The interband transition widths narrow, and their energies increase, resulting in optical absorption spectra which reveal struc-

ture indicative of discrete transitions (Fig. 3b) with gaps between transitions reaching several hundred meV. Crystal translational momentum which defines the energy dispersion relationship in bulk semiconductors and determines selection rules is relaxed. NC electronic states are often described within the  $\mathbf{k} \cdot \mathbf{p}$  formalism as Bloch wave functions modulated by an envelope function that is bounded by the surfaces of the NC, typically assumed to be a sphere. Neglecting spin-orbit interactions the resultant wavefunctions are labeled by two quantum numbers,  $n, L$  for the energy level and angular momentum, where orbitals are labeled according to angular momentum as  $S(L=0)$ ,  $P(L=1)$ ,  $D(L=2)$ , etc. In Fig. 3b,c we display a typical absorption spectrum of PbSe NCs and its second derivative. We assign the optical transitions according to the selection rules between symmetric wavefunctions determined by Kang and Wise [14, 32]; the first transition is the  $1S_e-1S_h$  transition, and the second transition has been a source of controversy [33, 34] because within the  $\mathbf{k} \cdot \mathbf{p}$  description this transition is assigned to a symmetry forbidden  $1S_e-1P_h/1S_h-1P_e$  transition. Each pair of states has a high level of degeneracy that increases

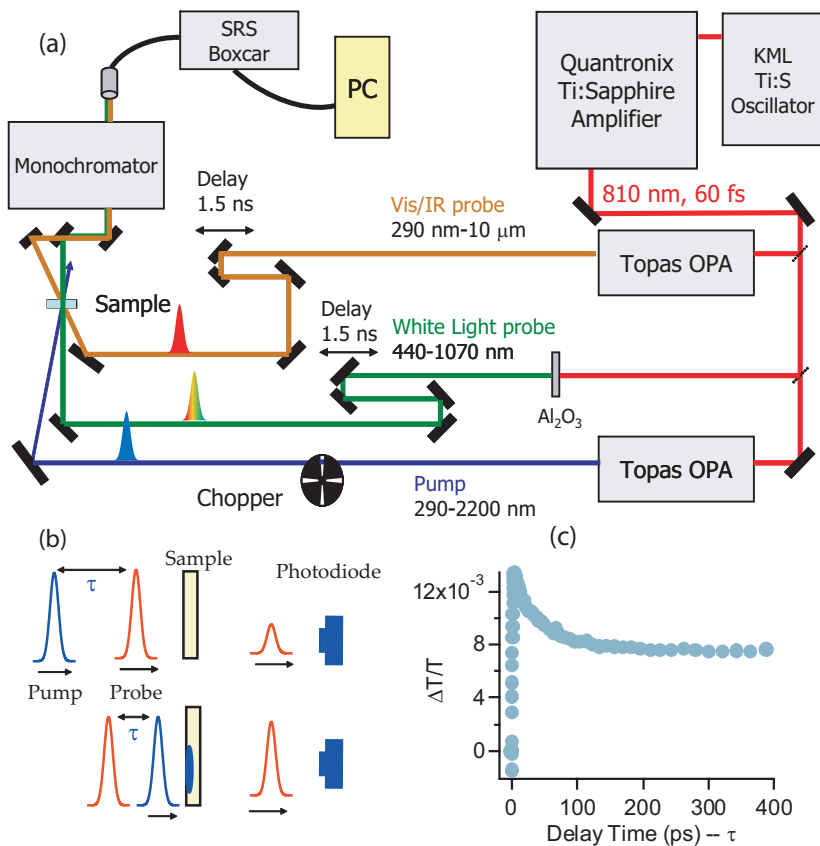


**Figure 4** (online color at: [www.lpr-journal.org](http://www.lpr-journal.org)) (a) Transient absorption spectrometer setup. An amplified Ti:sapphire laser emits 60 fs pulses at a 1 kHz repetition rate, determining the rate of sample pump and probe pulses from the independently tunable optical parametric amplifiers as well as the white light probe (2 mm-thick sapphire window). The system offers extensive tunability in the photoexcitation (pump, 290 nm–2.3 μm) and probe (290 nm–10 μm) beams, and the relative delay between pump and probe extends to 1.6 ns. A phase-locked optical chopper blocks every-other pump pulse, and the transmitted probe pulses are passed through a monochromator and detected (by Si, InGaAs, InSb, or HgCdTe photodetectors, depending on wavelength) to produce energy-scaled output pulses which are analyzed by a gated integrator for amplitude. (b) Schematic of a typical pump-probe experiment. The delay between the pump and probe pulses are controlled and the intensity of the transmitted pulse is measured as a function of the delay. (c) Example of data acquired via transient absorption technique, showing a photoinduced transmission bleach with ultrafast rise and partial signal decay.

with decreasing symmetry and that splits for (1) NCs with non-spherical shape, (2) surface passivation and reconstruction and (3) intervally interactions, resulting in P, D, etc. bands. The bands are further broadened by the sample size dispersion, which can be as low as a few percent. Atomistic calculations provide a deeper understanding of the nature of the electronic states. [35]

## 1.2. Femtosecond transient absorption

Femtosecond transient absorption spectroscopy (TA) monitors the change in transmission of a weak probe beam in response to an intense photoexcitation event. A typical TA apparatus (Fig. 4a) consists of an amplified Ti:Sapphire laser seeded by a wide bandwidth Ti:Sapphire oscillator. The amplified laser produces  $\sim 60$  fs FWHM pulses centered at 810 nm with a 1 kHz repetition rate, and pumps two independently tunable optical parametric amplifiers producing visible and NIR pulses for the respective pump and probe arms of the TA apparatus. The TOPAS allow for a wide tunability in both the pump (290 nm–2.3 μm) and probe (290 nm–10 μm) pulses. A white-light probe pulse can also be used, for which ultra-broadband pulses are generated in a 2 mm sapphire window. Passing the pump beam through a synchronous chopper phase-locked to the laser pulse train (500 Hz, blocking every other pump pulse) enables amplitude measurement of the transmitted probe

pulse with and without the pump pulse present. Comparison of the transmitted probe pulse energy with and without the pump permits calculation of the differential transmission,  $\Delta T/T_0$ . For small values of  $\Delta T/T_0$  and uniform excitation, we can relate this quantity to the change of the absorption coefficient,  $\Delta\alpha \cdot l = -\ln(\Delta T/T_0 + 1) \approx -\Delta T/T_0$ , where  $l$  is the pathlength. Fig. 4b is a schematic of a typical TA experiment. Varying the relative delay between pump and probe pulses enables measurement of the dynamics of the excited state created by the pump pulse (Fig. 4c). The pump spot size is controlled to be at least  $5 \times$  greater than the probe spot to ensure a uniformly excited area for the probe. When the sample strongly absorbs the pump light (high OD at  $\lambda_{\text{pump}}$ ), the photoexcited volume is not uniform. We discuss this situation below.

Following photon absorption by a semiconductor NC, the resulting electronic excitation consists of a conduction-band electron and a valence-band hole confined to the NC interior. This produces two measurable effects in the absorption coefficient of a typical semiconductor NC. Fig. 5 shows the linear (no photoexcitation) absorption spectrum overlaid with the absorption spectrum 100 ps after photoexcitation for a colloidal suspension of PbSe NCs with effective band gap at 0.94 eV. The first, or lowest-energy, exciton transition is bleached ( $\alpha$  decreases so that more light is transmitted), and also red-shifts slightly; in addition, a new absorption band appears in the infrared – for this sample the intraband absorption appears at  $\sim 0.3$  eV. The photoin-

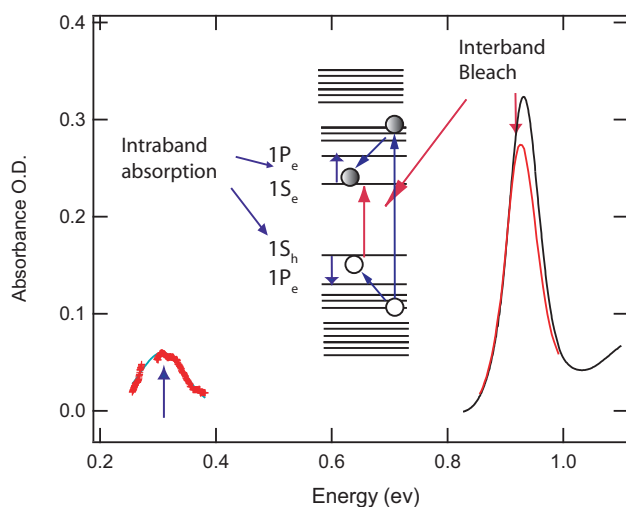


**Figure 5** (online color at: [www.lpr-journal.org](http://www.lpr-journal.org)) The origin of photoinduced absorption changes commonly measured to obtain the exciton population dynamics for a nanocrystal (NC) sample, depicted for the case where the valence and conduction band electronic structure are similar to one another. Following photoexcitation across the NC bandgap, the occupation of the  $|1S_e, 1S_h\rangle$  state results in a partial bleach of absorption of a probe pulse due to state-filling as well as a small red-shift due to a Stark effect. Thus, probing the absorption at the band edge energy, one observes a reduction in the absorption, i.e., a photoinduced bleach. If one probes the same sample with pulses tuned instead to the first intraband transition resonance (in this case, identically for electrons and holes due to symmetric electronic structure), the probe photons induce  $1S$ - $1P$  transitions and thereby measure a photoinduced increase in absorption. In this case the photoinduced absorption occurs at 0.3 eV (red crosses); there is a hole in the photoinduced spectrum that arises from absorption of light in the spectrometer.

duced bleach arises from state filling, or Pauli-blocking and the general interband photoinduced absorption change can be expressed as a sum over excitonic transitions as

$$\Delta\alpha(\hbar\omega) = \sum_i a_i G_i (\hbar\omega - \hbar\omega_i) (n_i^e + n_i^h) \quad (1)$$

where  $G_i$  is the unit-area absorption linewidth of the transition at  $\omega_i$ ,  $n_i^e$ ,  $n_i^h$  are the electron and hole occupation numbers, and  $a_i$  is proportional to transition  $i$ 's oscillator strength [36]. This is in contrast to photoluminescence which is sensitive to the product of the electron and hole occupation numbers. Changes in absorption may also occur due to Stark shifts resulting from the local charge distribution that modifies the electronic structure, or from photoionization and carrier trapping which may produce photoinduced absorption. For low excitation intensities where the average number of absorbed photons is less than  $\sim 2$ , for PbSe NCs, the measured  $\Delta T/T_0$  is linear in pump intensity for both interband bleaching and intraband absorption. Monitoring the recovery of the absorption as a function

of pump-probe delay time is directly proportional to the carrier population decay.

## 2. Background of multiple exciton generation

### 2.1. Carrier-carrier and carrier-lattice interactions in bulk semiconductors

Photon absorption by a bulk semiconductor crystal coincides with the interband transition of an electron from the valence band to the conduction band, and the simultaneous formation of a hole in the valence band. The binding energy of the electron-hole pair is too low to produce excitons at room temperature. Absorption of a photon with energy in excess of the semiconductor's band gap energy results in an electron and a hole, each with excess kinetic energy above their respective band edge (Fig. 6a). The total excess energy is shared to accommodate momentum conservation, such that the carrier with the lighter effective mass (typically the electron) receives most of the excess kinetic energy. The excess energy given to the electron is given by  $\Delta E_e = (h\nu - E_g)[1 + m_e^*/m_h^*]^{-1}$ . Since electrons and holes interact with the crystal lattice through the Fröhlich and deformation potential mechanisms, a population of electrons and holes form Fermi-Dirac distributions with well-defined electron- and hole-gas temperatures typically in thermal equilibrium with the lattice. However, following photoexcitation with a nearly monoenergetic ultrashort laser pulse (e.g.  $< 100$  fs pulsewidth) at photon energies exceeding the bandgap energy by at least  $kT$ , the initial distribution of electrons (or holes) is athermal and only forms a Fermi-Dirac distribution once inelastic carrier-carrier scattering has redistributed the electron energies to form a quasi-equilibrium distribution exhibiting temperatures above that of the lattice. For example, in GaAs, the fastest process affecting the energy of a hot electron is inelastic carrier-carrier scattering, occurring on a timescale as short as  $\sim 10$  fs [37]. Hot charge carriers interact with the crystal lattice primarily through LO-phonon emission on the  $\sim 100$  fs timescale (electron-phonon scattering rate of  $\sim 10^{13} \text{ s}^{-1}$ ), losing energy to the crystal lattice in the form of heat until the carrier distribution temperature matches the lattice temperature [38, 39].

As the excess energy of an electron increases above the band edge (Fig. 6b), the electron-phonon scattering rate also increases [40]. For cases where either the electron or the hole attains kinetic energy in excess of the semiconductor's bandgap energy, the charge carrier has sufficient energy to scatter with a valence band electron, boosting it across the bandgap to the conduction band. In this process, known as impact ionization (I.I.), an initially hot carrier converts some of its energy to a second electron-hole pair while relaxing back toward its respective valence or conduction band edge. Although I.I. is often discussed in ref-

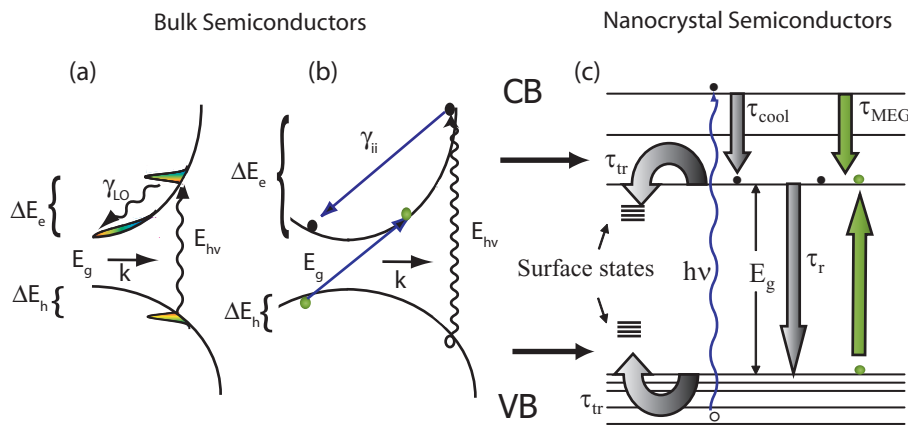


**Figure 6** (online color at: [www.lpr-journal.org](http://www.lpr-journal.org)) (a) Initial photo-excited carrier dynamics in bulk semiconductors. Following excitation by a femtosecond laser pulse with total energy in excess of the band gap, an athermal electron and hole population is formed with excess kinetic energy. The electrons/holes thermalize and cool to form a Fermi-Dirac distribution at the band gap (no excess kinetic energy) on the timescale of  $\sim 100$  fs. (b) Electrons/holes with excess energy of greater than  $E_g$  may undergo impact ionization (I.I.) to form additional carriers at the band gap. The I.I. event must satisfy both energy and momentum conservation. (c) For semiconductor NCs the nature of the conduction and valence bands changes due to the quantum confinement and carrier relaxation processes are also modified. Photoexcitation at energies in excess of the band gap results in carriers with excess energy defined by the particular absorption selection rules of the nanocrystals. Surface traps are more important in NCs due to the increased surface to volume ratio. Cooling by phonon emission occurs less efficiently, and carrier multiplication (MEG) also is modified.

erence to electrons accelerated by an applied electric field to high kinetic energies exceeding the ionization threshold (e.g., within an avalanche photodiode), sufficiently energetic photogenerated carriers can also impact ionize to generate additional electron-hole pairs. Like all scattering processes occurring in bulk crystals, impact ionization requires that both energy and momentum be conserved. Within the constructs of electronic band structure, these conservation requirements, pertaining to both the electron-hole pair photogeneration and impact ionization processes, elevate the photon energy threshold for impact ionization above the simple  $2E_g$  level. For parabolic bands the *excess* energy threshold for an electron to undergo I.I. while satisfying momentum and energy conservation is given by  $\Delta E_e = (2m_e^* + m_h^*) E_g / (m_e^* + m_h^*)$  [41]. Bulk PbS has  $m_e^* \approx m_h^*$  and thus the excess energy threshold becomes  $\Delta E_e \approx 3E_g/2$ . For photoexcited carriers created such that the photon energy is divided among the electron and hole as described above, the I.I. onset occurs at  $h\nu \sim 4E_g$  and both the electron and hole would have the necessary excess energy to undergo I.I. The exact I.I. threshold depends on the specific band structure (which deviates from parabolic at high energies) as well as the presence of additional nearby bands. Impact ionization must also compete with carrier cooling and as a result the threshold for I.I. is higher than expected from purely momentum and energy conservation arguments, for example, in bulk PbS it was found to be  $\sim 4.5E_g$  in one experiment [42]. For silicon, which has been the subject of extensive theoretical modeling as well as numerous electronic and optical measurements, the threshold for the onset of I.I. by photogenerated carriers is  $\sim 3.1$  eV, as borne out by several experimental

studies [7, 43–46]. Together with the influence of silicon's band structure, energy relaxation through phonon emission also reduces the efficiency of impact ionization.

The case of bulk GaAs offers some quantitative scattering rate information based on both experiment and theory. When the excited carrier density exceeds about  $1 \times 10^{17} \text{ cm}^{-3}$ , enhanced carrier-carrier scattering with a rate of  $\sim 4 \times 10^{13} \text{ s}^{-1}$  results in thermalization on a timescale of  $\sim 100$  fs [37, 47, 48]. In comparison, polar optical phonon emission is largely independent of the carrier density and occurs in bulk GaAs with a rate of  $\sim 6 \times 10^{12} \text{ s}^{-1}$  [48]. A full band Monte Carlo simulation of impact ionization in GaAs showed that for increasing excess energy above the band gap, the electron impact ionization scattering rate surpasses the total phonon scattering rate only when the electron kinetic energy exceeds  $\sim 5$  eV [40].

For typical solar-photogenerated carrier energies, I.I. does not occur in bulk semiconductors with sufficiently high rate to compete with carrier cooling via phonon scattering. As a result, hot carriers in solar cells lose energy predominantly through phonon scattering, i.e., through inelastic collisions which transfer some of the charge carrier's kinetic energy to the lattice resulting in heat. As noted above (see Fig. 7), *c*-Si does not show significant impact ionization for photon energies within the range of the solar spectrum [46, 49]. Device modeling indicates that a hypothetical *c*-Si solar cell, operating with efficient impact ionization such that every absorbed photon at or above  $2E_g$  produced two electron-hole pairs, would reduce the power loss to heat from 47% to 39% while increasing the electrical power from 33% to 41%.

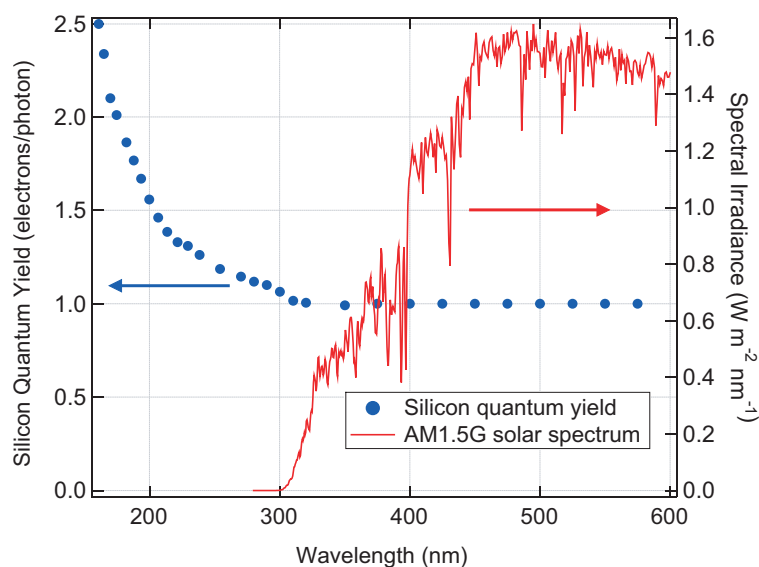


**Figure 7** (online color at: [www.lpr-journal.org](http://www.lpr-journal.org)) The wavelength dependence of the quantum yield for a UV-optimized Si p-n junction photodiode (left axis) compared to the standard (terrestrial) AM1.5G solar spectral irradiance (right axis), showing the inefficacy of impact ionization for conventional Si solar cells. Silicon quantum yield data compiled from Applied Optics **26**, 5284 (1987) and Metrologia **35**, 329–334 (1998).

## 2.2. Carrier cooling in semiconductor NCs

Since the primary mechanism for rapid cooling of hot carriers is optical phonon emission, NCs with gaps of 100 meV or more between intraband transitions require the simultaneous emission of multiple phonons (typical optical phonon energy of  $\sim 30$  meV), or the participation of very high-energy phonon modes, such as surface or molecular modes [27], to allow efficient cooling to the lowest energy levels. The expected inhibition of electronic relaxation in the presence of sparse electronic structure is referred to as the phonon bottleneck (not to be confused with the hot phonon bottleneck [50], which refers to highly non-equilibrium phonon populations which at high excitation density slows cooling in semiconductor quantum wells [38]). Several experiments have shown that in fact the electron cooling rate remains relatively fast in NCs, an observation which has been explained by an Auger-like cooling process in which the electron can relax by scattering its energy to the hole, which in turn cools efficiently through the more dense manifold of valence band states [23]. Evidence exists for slowed carrier cooling in NCs when the electron and hole are partially separated through, e.g., surface trapping of one of the carriers [26, 27].

One expects a slower cooling rate in smaller dots due to the increased spacing of electronic levels and concomitant strengthening of the phonon bottleneck. However, the opposite trend is observed experimentally—the cooling rate increases as the size of the NCs decreases. In Fig. 8a we show relaxation from the P to S state in a series of InP NCs and observe that the relaxation rate increases as the NC size decreases (Fig. 8b). A similar trend has also been reported for CdSe NCs [51]. In agreement with these reports the relaxation rate in CdSe rods is faster in thinner rods of similar length [52]. From these reports we conclude that the relaxation occurs via a different mechanism than in bulk. Efros et al. proposed the Auger cooling mechanism (*infra*

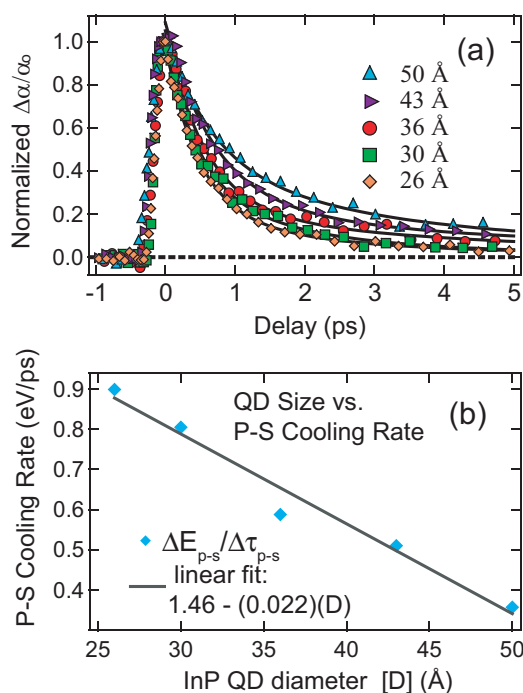


**Figure 8** (online color at: [www.lpr-journal.org](http://www.lpr-journal.org)) Electron cooling dynamics as a function of InP NC size. (a) Normalized recovery of 1S bleaching following re-excitation of 1S electron to 1P level for five InP NC samples with different mean diameters. Symbols are data and solid lines are bi-exponential fits. (b) Average 1P-to-1S cooling rate vs. NC diameter for the same five InP NC samples.

*supra*) [26], and relaxation is faster in the smaller dots due to an increase in the electron-hole Coulomb interaction. In a recent time-resolved THz study both the electron and hole relaxation rates were measured in CdSe NCs and direct evidence was found supporting the Auger cooling mechanism [53]. In Pb-salt NCs the Auger cooling mechanism is

not operative because the effective mass of the electron and hole are roughly equal and therefore we expect a phonon bottleneck in both the valence and conduction bands. Harbold et al. found that carrier relaxation is slower [54] in PbSe NCs compared to InP and CdSe but the relaxation rate is still larger than expected from a true phonon bottleneck and increases with decreasing NC size. Blackburn et al. measured P-to-S relaxation rates in charged InP NCs and found that electrons in the absence of core-confined holes cooled more slowly, unable to exploit the Auger cooling mechanism [26]. Nonetheless, cooling remained relatively fast ( $\sim 3$  ps), indicating that in the absence of the e-h Auger mechanism, electrons follow other slightly less efficient cooling routes. A complete understanding of cooling in NCs that is consistent with all experimental observations is still lacking [55]. A recent calculation of carrier relaxation in PbSe NCs based upon a time-dependent density functional theory [35] found that the density of states is much greater than what is typically assumed, but that most of these states are dark and do not contribute to the absorption spectrum. These dark states are coupled to light states via a variety of NC vibrations (phonons) and can therefore participate in carrier relaxation. While the calculation was done for only one size NC and therefore no size-dependent results were reported, these calculations are the most extensive to date and provide new insight to carrier relaxation in NCs.

Strong carrier-carrier interactions are also expected to occur within photoexcited NCs, supporting the possibility of an enhanced rate of impact ionization. At elevated carrier densities, the carrier-carrier scattering rate increases, and since typical effective volume carrier densities within a photoexcited colloidal nanocrystal frequently exceed  $10^{19} \text{ cm}^{-3}$  for a single exciton, strong carrier-carrier interactions are expected. In addition, the electronic excited state wavefunction can extend beyond the nanocrystal into the lower-dielectric-constant capping molecule and solvent, reducing the carrier-carrier screening effects below that for bulk crystals and enhancing carrier-carrier interactions.

### 2.3. Poisson statistics and Auger recombination

Due to the quantized nature of photon absorption within NCs (i.e., absorption of integral numbers of photons from a single laser pulse), NC samples offer a unique system for the study of carrier-density-dependent exciton-exciton interactions – i.e., Auger recombination, in which an electron-hole pair recombines nonradiatively and imparts the original energy to a third charge carrier, either an electron or a hole. The Auger recombination rate for an intrinsic bulk semiconductor depends on the cube of the carrier density. The presence of two excitons within a NC of diameter 5 nm coincides with a volume carrier density of  $1.3 \times 10^{19} \text{ cm}^{-3}$ , a density typically sufficient to induce a high rate of Auger recombination [56]. For pulsed laser excitation of a solution of NCs with pulses of sufficiently short duration that no carrier recombination occurs during excitation, the fraction

$P_m$  of NCs within the excitation volume with  $m$  photogenerated excitons varies with Poisson statistics as

$$P_m = \frac{\langle N_0 \rangle^m}{m!} e^{-\langle N_0 \rangle} \quad (2)$$

where  $\langle N_0 \rangle$  is the average number of photons absorbed per NC per pulse, given by  $\langle N_0 \rangle = \sigma_a \cdot j_p$ , with a per-NC absorption cross section of  $\sigma_a$  ( $\text{cm}^2$ ) and a photon pump fluence ( $\text{photons} \cdot \text{cm}^{-2} \cdot \text{pulse}^{-1}$ ) [30]. Thus, pulsed laser excitation enables the controlled study of photoexcited NC samples with varying numbers of photons absorbed, i.e., by careful control of the laser beam spot size and the pulse energy, one can control the excitation level for a sample of NCs to produce populations of photoexcited NCs heavily weighted toward  $m = 1$  (e.g.  $\langle N_0 \rangle < 0.25$ ) with almost no NCs excited at or above  $m = 2$ , or shift the average NC excitation level higher (e.g.  $\langle N_0 \rangle \approx 2$ ) to produce large populations of NCs with  $m \geq 2$ . Klimov et al. conducted time-resolved photoinduced bleach measurements on a solution of colloidal CdSe NCs, varying  $\langle N_0 \rangle$  to study the exciton population decay dynamics as a function of the per-NC excitation level. Their data indicated good agreement with an Auger recombination model such that the lifetime  $\tau_m$  of an  $m$ -exciton state varies as  $C_A(m/V_{\text{NC}})$  for  $m \geq 2$  where  $C_A$  is a size-specific ‘‘Auger constant’’ and  $V_{\text{NC}}$  is the NC volume [30]. However, the ‘‘Auger constant’’ varies as  $R^3$  for varying NC radii, indicating a unique size-dependent nature for Auger recombination in CdSe NCs. The Auger interaction is referred to as strong within quantum confined NCs not necessarily because Auger recombination proceeds more quickly in NCs than in a bulk semiconductor with an equivalent volume carrier density, but rather due to the dominance of Auger recombination for NCs excited with two or more excitons [57]. Fig. 9 shows values for the Auger coefficient reported for several bulk semiconductors as well as for NCs of PbSe and Si with different sizes, and thus different blue-shifted bandgaps. Narrower bandgap semiconductors have larger Auger coefficients, indicative of faster Auger recombination for a given carrier density; in contrast, larger bandgap semiconductors show relatively inhibited Auger recombination. Interestingly, the relationship appears to hold for the size-dependent bandgaps of PbSe NCs, such that smaller NCs of a given material show slower Auger recombination for a given volume carrier density. The relationship may not hold, however, for blue-shifted Si NCs relative to their bulk counterpart. Additional studies are needed to ascertain clear dependences of the Auger recombination rates on bandgap for NCs, but the size-dependent bandgap likely accounts for the reported size-dependent Auger reported for CdSe NCs [30]. Characterization of Auger interaction strength varying with NC size is complicated by size-dependent effective bandgap as well as other changes in electronic structure.

Single exciton lifetimes depend much more on the dipole transition strength and the NC surface properties, and range from  $\sim 20$  ns for CdSe NCs to  $\sim 2$   $\mu\text{s}$  for PbSe or PbS NCs. Auger recombination limits the lifetime of the

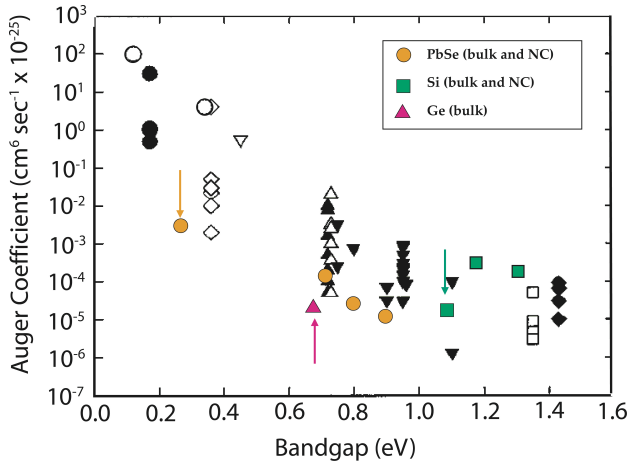


**Figure 9** (online color at: [www.lpr-journal.org](http://www.lpr-journal.org)) Auger coefficient versus semiconductor bandgap energy. Values shown for bulk III-V compound semiconductors, ( $\blacklozenge$ ) GaAs, ( $\square$ ) InP, ( $\blacktriangle$ ) GaSb, ( $\bullet$ ) InSb, ( $\diamond$ ) InAs, ( $\nabla$ ) InGaSb, ( $\circ$ ) InGaSb, ( $\triangle$ ) InGaAs (experimental and calculated values, including the effects of varying the doping level) were extracted from [96], the values for Si and Ge were taken from the online NSM archive [97], and the value for bulk PbSe comes from an average of [98] and [99]. The NC values were calculated from experimental data based on the NC volume and the biexciton lifetime measured in our lab by transient absorption spectroscopy. Arrows indicate the bulk Auger coefficient values for Ge, Si, and PbSe.

two-exciton (biexciton) state for typically-sized (e.g., diameters of 2 nm to 8 nm) colloidal NCs to the range of  $\sim 10$  to  $\sim 100$  ps, depending on semiconductor material and the NC size. Multiple excitons within a single NC undergo Auger recombination, at rates which increase as the number of excitons increases. For example, for  $k \geq 2$  excitons, the Auger recombination rate for a QD with  $k$  excitons to decay to  $(k - 1)$  excitons varies as:  $\tau_k^{-1} \propto k^2$ . Therefore, the values for  $\tau_k$  can be determined by measuring the aggregate population decay dynamics as a function of average excitation level,  $N_0$ . As a result of the nonradiative Auger recombination the probabilities  $B_k(t)$  are determined by the following system of kinetic equations, where  $B_k(t)$  represents the probability of finding  $k$  excitons in a QD at time  $t$  after photoexcitation:

$$\begin{aligned} \frac{dB_k}{dt} &= -\frac{B_k}{\tau_k}, \quad \frac{dB_{k-1}}{dt} = -\frac{B_{k-1}}{\tau_{k-1}} + \frac{B_k}{\tau_k}, \dots, \quad \frac{dB_1}{dt} \\ &= -\frac{B_1}{\tau_1} + \frac{B_2}{\tau_2}. \end{aligned} \quad (3)$$

In the limit where  $\tau_{k+1} \ll \tau_k$ , the solution to Eq. 2 simplifies to a sum of exponentials,

$$n(t) = \sum_{k=1}^{\infty} A_k \exp(-t/\tau_k) \quad (4)$$

where the  $A_k = \sum_{j=k}^{\infty} B_j(0)$  and where  $B_k(0)$  are the initial values of these probabilities. In our case, the single exciton lifetime  $\tau_1$  is estimated to be  $\sim 50\tau_2$ . In general for higher multiplicities the condition  $\tau_{k+1} \ll \tau_k$  ( $k > 1$ ) does not hold, but Eq. 3 is still good approximation to Eq. 2 for  $\langle N_0 \rangle < 2$ . Note that the  $A_k$  pre-factors reflect the fact that all QDs with  $k$  excitons undergo Auger recombination until they reach the single exciton state ( $k = 1$ ). A more accurate analysis of the multiexciton dynamics in nanostructures has recently been reported [58] based on a stochastic model rather than a bulk model. The analysis described here provides an excellent approximation to that analysis when  $\tau_1 \gg \tau_2$  and  $\langle N_0 \rangle < 2$ . The stochastic analysis does not affect the derived MEG QYs. In the absence of MEG ( $h\nu < 2E_g$ ), the initial values are determined by Poisson statistics:  $B_k(0) = P(k)$ ,  $B_{k-1}(0) = P(k-1)$ ,  $\dots$ ,  $B_1(0) = P(1)$ , i.e., the probability of directly creating  $k$  excitons in a QD by absorption of  $k$  photons.

In Fig. 10a, we show carrier dynamics for 4.7 nm PbSe NCs excited at  $1.5E_g$  (below MEG threshold) and probing the intraband photoinduced absorption. The pump photon fluence is varied to obtain  $\langle N_0 \rangle$  values ranging from 0.26 to 1.89. A global fitting routine was employed to simultaneously fit the AR model described above to the three data sets where only  $\tau_2$ ,  $\sigma_{\text{Pump}}$ , and an overall scaling parameter related to the photoinduced absorption cross section are varied globally to produce the fits shown as solid lines, the single exciton lifetime is held fixed at 6 ns. We find that the biexciton lifetime is 110 ps for this data set. We have done this analysis for a variety of PbSe and Si NC sizes and display our results in Fig. 10b overlaid with the CdSe NC biexciton lifetime data from [30]. We find that our results vary approximately linear with the volume of the NCs. The posited scaling of Auger processes with  $\sim R^{-3}$  favors strong carrier-carrier interactions in NCs [19], consistent with the proposition for enhanced impact ionization, a closely-related carrier-carrier scattering process [5, 12].

#### 2.4. Multiple exciton generation measurement and analysis

Following photoexcitation by a short laser pulse (width  $\sim 200$  fs), the time-dependence of the average exciton population per NC can be measured by monitoring (a) the bleaching of the bandedge (first exciton) transition (reduced absorption, due to state-filling), (b) the photoinduced absorption at intraband transition energies (Fig. 5), (c) time-resolved terahertz spectroscopy (TRTS) which monitors intraband hole transitions for large effective mass semiconductors such as InAs, or (d) time-correlated single photon counting (TCSPC) – as demonstrated for CdSe NCs [59]. The signature of MEG is the appearance of a fast multiexciton decay component with the identical time constant as AR when photoexciting above the energy conservation threshold for MEG ( $> 2E_g$ ) and at low intensity so that each photoexcited NC absorbs at most one photon. Results

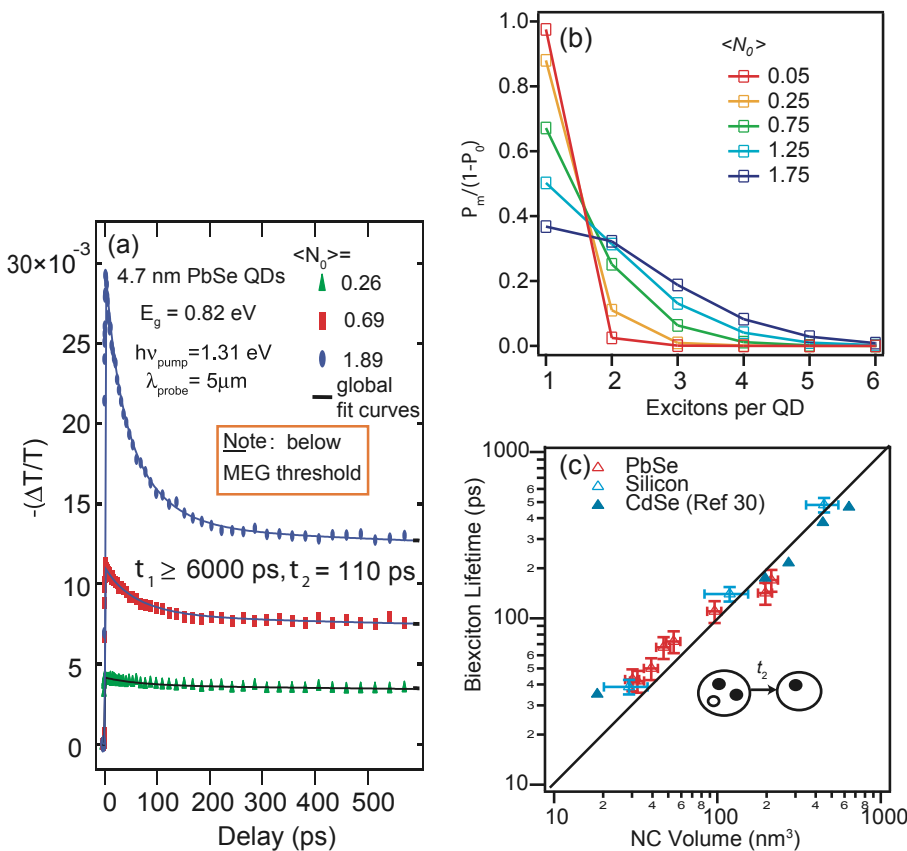


**Figure 10** (online color at: [www.lpr-journal.org](http://www.lpr-journal.org)) (a) Exciton population decay dynamics in PbSe NCs as a function of the initial average exciton number,  $\langle N_0 \rangle$ . In contrast with the long single-exciton lifetime observed for this PbSe NC samples, the Auger recombination of multiexciton states occurs on the  $\sim 100$  ps timescale and is clearly evident for values of  $\langle N_0 \rangle$  exceeding  $\sim 0.5$ . (b) Variation of the number of photons  $m$  absorbed per nanocrystal (NC) from an ultrashort laser excitation pulse follow Poisson statistics. The graph shows the fraction of photoexcited NCs absorbing  $m$  photons as a function of the average per-NC photon absorption number,  $\langle N_0 \rangle$ . (c) Aggregate data from several reports of the biexciton lifetime ( $t_2$ ) variation with NC size and material. Note the approximate universality observed for the linear dependence of the NC volume versus  $t_2$  for NCs of Si, PbSe, and CdSe. The black line represents a linear dependence of  $t_2$  with NC volume.

of measurements based on (a) and (b) have been shown to yield identical results for PbSe NCs in solution [14]. In addition to ultrafast spectroscopic techniques, a quasi-cw photoluminescence technique based on nanosecond laser pulses enables the observation of multiexciton states through analysis of the spectral signature for biexciton radiative emission [60, 61]. The majority of reports of MEG have been based on ultrafast transient absorption and emission techniques. The first TCSPC-based measurements, reported by Schaller et al. [59] and conducted on CdSe NCs, demonstrated the equivalence of results obtained via TCSPC to those measured using ultrafast transient absorption. In addition, the CdSe TCSPC data revealed a spectral signature assigned to emission from biexciton state; these data resulted from excitation at the extremely low value of  $\langle N_0 \rangle = 0.001$ . Contradicting the CdSe results reported by Schaller, a report from Nair et al. also utilized time-resolved PL and found no evidence of significant MEG for CdSe and CdTe NCs following photoexcitation up to  $h\nu > 3E_g$  [62]. In the case of work from Pijpers et al. on InAs core-shell NCs [61], the authors originally published positive MEG results using three different techniques but subsequently raised concerns about their results in a recently-published correction [61].

Any alternative process that can explain the appearance of the fast AR decay component at high photon energies and low photon fluences must be consistent with the following experimentally determined observations: (1) the dynamics

are the same as AR, showing the same decay rate and dependence on NC volume; (2) the fast component with time constant equal to that of AR steadily increases with photon energy with an onset greater than  $2E_g$ ; and (3) the effect remains at low excitation fluences. Faster decays can be observed in bulk semiconductor as a function of decreasing wavelength due to fast surface recombination. However, for nanocrystals the distance scale per NC is so small that recombination at surface states should not depend on generation depth and hence excitation wavelength as observed here. Resonant energy transfer (RET) of an exciton from one NC to another NC which already has an exciton can produce a single- to multiexciton transition, thereby creating multiexcitons per absorbed photon. However, the rate of RET would decrease at low photon fluences, in contrast to what is observed, although this effect might be expected to increase with decreasing wavelength due to the higher OD at lower wavelengths. Surface recombination into a continuum of high energy states would need to be much faster than the dynamics observed here to compete with carrier cooling and thus not have the AR time constant. Similarly, fast transient absorption from impurities excitable only at high photon energies would not show a steady amplitude increase with decreasing excitation wavelength and would not have identical band-edge bleaching and intraband absorption dynamics, as observed.

We now describe how we analyze the quantum yield (QY) based on the decay of multiexciton states in QDs.

The QY is the average number of excitons created by one absorbed photon. As described above, multiple excitons within one NC undergo Auger recombination and therefore exhibit reduced lifetimes. The presence of MEG can be observed through analysis of the shape of the population decay curve, at delay times longer than all MEG and cooling processes. When MEG does occur, there are additional contributions to the amplitudes for  $k > 1$ . By analyzing these additional contributions, we can determine the QY. We first determine the  $A_k$ 's and  $\tau_k$ 's (Eq. 3) under conditions where MEG *does not occur* (e.g.,  $h\nu < 2E_g$ ), that is, the case for which the  $A_k$ 's depend solely on the photon fluence and the NC absorption cross section. Since we can measure the photon fluence this determines the cross section. The absorption cross section is linearly related to the sample's optical density (OD);  $\sigma \cdot N_{\text{QD}} = \text{OD} \cdot \ln(10)$ . By determining  $\sigma$  at wavelengths below the MEG threshold we implicitly determine it at shorter wavelengths.

Multiple exciton generation results in QY values greater than one. In our analysis we assume that each absorbed photon creates one or more excitons, excluding other possible processes such as NC ionization. We ensure not to analyze any data where  $\Delta T/T_0$  is non-linear with photon fluence. For this analysis we treat the MEG event as instantaneous. For photoexcitation in the range where  $2E_g < h\nu < 3E_g$ , energy conservation permits only one particle of an electron-hole pair to produce an additional exciton; i.e., the maximum QY is 2. We define  $\eta$  as the probability of an exciton producing an additional exciton through MEG. There are two possible scenarios for a NC absorbing one photon such that  $2E_g < h\nu < 3E_g$ : no MEG occurs (probability of  $1 - \eta$ ), or MEG does occur (probability of  $\eta$ ). For a NC absorbing two photons within the energy range  $2E_g < h\nu < 3E_g$ , there are four possible scenarios and so forth. The additional terms due to MEG that contribute to  $A_k$  (deviate from Poisson statistics) for  $2E_g < h\nu < 3E_g$  are,

$$\begin{aligned} A_1 &= \sum_{k=1}^{\infty} P(k); \\ A_2 &= \sum_{k=2}^{\infty} P(k) + P(1) \cdot \eta; \\ A_3 &= \sum_{k=3}^{\infty} P(k) + P(2) \cdot (2\eta(1 - \eta) + \eta^2) \end{aligned} \quad (5)$$

where  $P(k)$  accounts for directly generated excitons (Poisson contribution). In the region where  $3E_g < h\nu < 4E_g$ , energy conservation permits both the carriers of an electron-hole pair to produce an additional exciton; i.e., one exciton has two "chances" to produce an additional exciton; we treat the chances as independent of one another. Consistent with the region where  $2E_g < h\nu < 3E_g$ , we define  $\eta$  as the probability of an exciton succeeding in one chance to produce an additional exciton through MEG, and we define the probability that an exciton fails, in one chance, to

produce an additional pair as  $(1 - \eta)$ . The probability of producing two additional pairs is given by  $\eta^2$ . In analogous fashion, for  $3E_g < h\nu < 4E_g$  the first few  $A_k$  terms with MEG included are,

$$\begin{aligned} A_1 &= \sum_{k=1}^{\infty} P(k); \\ A_2 &= \sum_{k=2}^{\infty} P(k) + P(1) \cdot (2\eta(1 - \eta) + \eta^2); \\ A_3 &= \sum_{k=3}^{\infty} P(k) + P(2) \cdot \sum_{j=1}^4 \eta^j \cdot (1 - \eta)^{4-j} ({}_4C_j) \end{aligned} \quad (6)$$

where  ${}_4C_j$  is the combinatorial function with  ${}_nC_r = n!/(r!(n-r)!)$ . When fitting our data, we extend the sum in Eqs. 4 and 5 to include events originating from those NCs absorbing three or fewer photons. The quantum yield is given by  $QY = 1 + \eta$  for the region  $2E_g < h\nu < 3E_g$ , and by  $QY = 1 + 2\eta$  for the region  $3E_g < h\nu < 4E_g$ .

Transients are collected for a variety of pump photon energies while ensuring that we maintain a constant  $\langle N_0 \rangle$  at the front of the sample. Since  $\langle N_0 \rangle$  scales with both incident pump photon fluence and the absorption cross section, we adjust the incident pump photon fluence according to the linear O.D. of the sample. Eq. 3 is then fit to the resulting transients, substituting the coefficients  $A_k$  provided in Eqs. 4 or 5, which include MEG. A global fitting routine is once again employed, however in this case we hold constant  $\langle N_0 \rangle$  and the biexciton lifetime  $\tau_2$  and allow  $\eta$  to vary. Fig. 11 displays a typical experiment to determine MEG in this fashion. Fig. 11a is the linear absorption spectrum and we have overlaid arrows indicating the different pump wavelengths employed. The TA data are displayed in Fig. 11b with the results of the global fitting shown as solid black lines. An additional scaling factor is applied to each data set because as the OD increases, the total number of NCs excited decreases so that a constant density of excited carriers is maintained within the excited volume (which decreases); this implies that  $\Delta T/T$  becomes much smaller. There are two adjustable parameters: the QY which determines the shape of the transients, and a scaling factor. The inset in Fig. 11b displays the best fit QYs for the data set. The method we have presented here does not depend on the  $\langle N_0 \rangle$  as we explicitly account for contributions to the decay from any NCs that absorbed more than two photons. However, to ensure that higher non-linear effects do not complicate our results we always collect data for  $\langle N_0 \rangle < 0.5$ . Note that in other treatments to determine the QY the transients are all normalized at pump-probe delays longer than the AR time where only single excitons remain, and we have presented the data in this fashion.

To improve the signal-to-noise ratio of our measurements and to ensure that we are in the single exciton limit we have developed a simple technique that requires measuring the transient absorption at only three pump-probe delays rather than collecting the entire trace for a variety

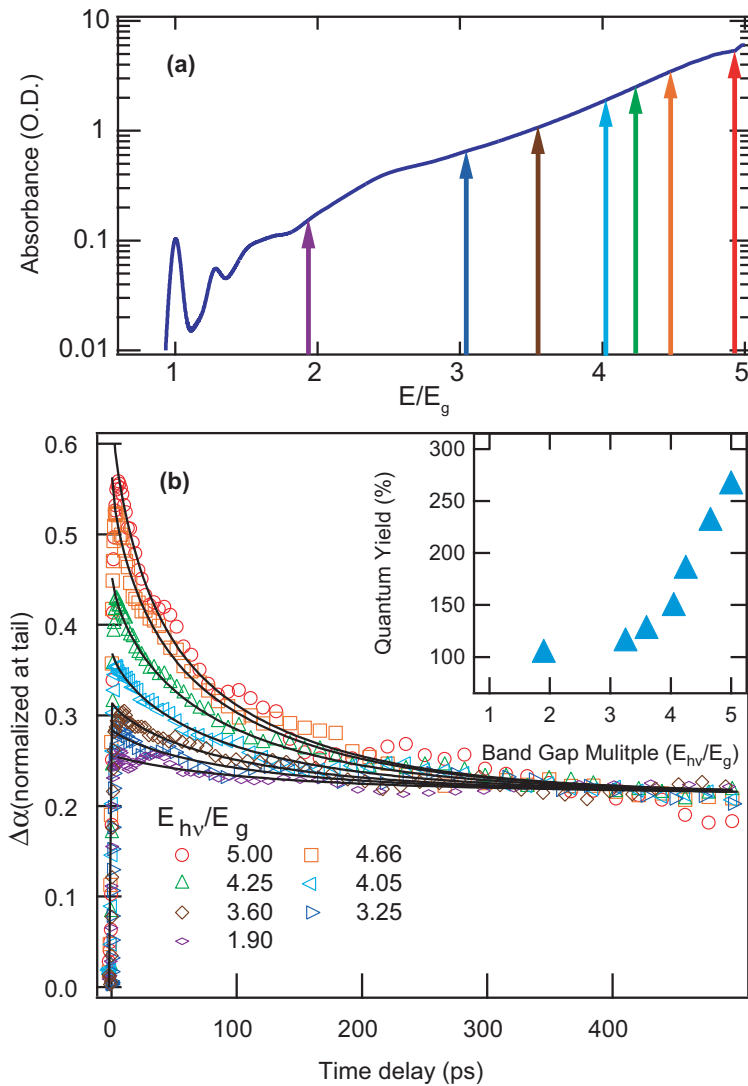


**Figure 11** (online color at: [www.lpr-journal.org](http://www.lpr-journal.org)) (a) The linear absorption of PbSe NCs, with the energy axis labeled in quanta of the bandgap. Colored arrows indicate the excitation energies for population decay curves presented in (b). The average per-NC excitation level was held at  $\langle N_0 \rangle = 0.25$ . Global fitting of the seven traces enables extraction of QY data as described in the text. Inset shows QY vs. incident photon energy.

of pump powers. Furthermore this method allows for the extraction of  $\sigma_{\text{pump}}$  with higher accuracy. This is especially important when the linear absorption spectrum may not be linearly related to the absorption cross section, which occurs when measuring films of NCs where wavelength dependent scattering may be important. In addition, for NC films that exhibit some degree of electronic coupling,  $\sigma_{\text{pump}}$  maybe be modified due to a wavelength dependent dielectric screening [63]; therefore,  $\sigma_{\text{pump}}$  is not known *a priori* based on that of the isolated NCs.

The number density of absorbed photons,  $N_{\text{ex}}$ , is equal to  $N_{\text{ex}} = J_0 [1 - \exp(-\sigma_{\text{pump}} N_{\text{NC}} l)] / \beta$  where  $J_0$  is the photon fluence at the front of the cuvette,  $\beta$  is the absorption depth,  $\sigma_{\text{pump}}$  is the absorption cross section at the pump wavelength,  $N_{\text{NC}}$  is the density of NCs in solution and  $l$  is the cuvette pathlength, here the absorption coefficient is  $\alpha_{\text{pump}} = \sigma_{\text{pump}} N_{\text{NC}}$ . We consider two limiting cases: 1) high OD at the pump wavelength and 2) low OD at the pump wavelength. Under these two conditions, we will have different values of  $\beta$ :  $\beta = l$

at low OD and  $\beta = 1/\alpha_{\text{pump}}$  at high OD. The differential transmission for photoinduced bleach or absorption is  $\Delta T/T = \exp(\sigma_{\text{probe}} N_{\text{ex}} l) - 1 \approx \sigma_{\text{probe}} N_{\text{ex}} l$ , where we have introduced the absorption cross section at the probe wavelength,  $\sigma_{\text{probe}}$ , and  $N_{\text{ex}}$  is the photoexcited number density, given above.

For pump-probe delay times much greater than the Auger decay time, any NCs that absorbed more than one photon will undergo AR to yield one exciton per excited NCs. We can calculate the number of excited NCs assuming Poisson statistics as  $N_{\text{ex}} = N_{\text{QD}} [1 - \exp(-J \bullet \sigma_{\text{pump}})]$ . We define the ratio of the transient absorption at short and long pump-delays as  $R_{\text{pop}}$  and find that, including the MEG-QY and a term accounting for any single exciton decay,

$$R_{\text{pop}} = \frac{J_0 \sigma_{\text{pump}} \delta \cdot QY}{(1 - \exp(-J_0 \sigma_{\text{pump}}))} \quad (7)$$

where  $\delta = \exp(t_{\text{late}} - t_{\text{early}}) / \tau_1$  accounts for any single exciton decay. We find that this ratio holds exactly in the low

OD limit. In the high OD limit, the excitation volume is not uniform and Poisson statistics do not hold when considering the entire excitation volume. In this situation, Eq. 6 can still be employed to determine the QY, though  $\sigma_{\text{pump}}$  will be underestimated. We can easily account for this by a numerical calculation accounting for the non-uniform excitation volume, including explicitly the average number of excitons/NC as a function of distance into the sample. This situation has also been addressed in a recent publication on InAs/CdSe/ZnSe core/shell1/shell2 nanocrystals [64].

Silicon NCs present a unique challenge to measuring the QYs due to the absence of a well defined first exciton transition (we therefore measure intraband photoinduced absorption) [65]. Optical transitions at the band-edge are not allowed and there is a large difference in  $\sigma_{\text{pump}}$  for above and below the MEG threshold (the ratio can be as great as  $\sim 700$ ). The  $R_{\text{pop}}$  measurement improves the SNR in two ways, (1) we only need to collect  $\Delta T/T_0$  at three delays, a short delay, a long delay ( $t > 3\tau_2$ ) and at a negative delay and (2) we collect the data for a variety of intensities at one pump wavelength so that we can ensure we have reached the single excited exciton level. Using Eq. 6, we fit all of the intensities. As a check we determined  $\sigma_{\text{pump}}$  of 3.8 nm diameter Si NCs at low OD and find that  $\sigma(2.70 \text{ eV}) = 2.3 \times 10^{-16} \text{ cm}^2$ , which compares well that reported previously ( $\sim 2.0 \times 10^{-16} \text{ cm}^2$ ) for this size of Si NC [66]. The value also compares favorably with the screened bulk absorption coefficient [65]. For the above-MEG threshold (blue squares in Fig. 12) we hold fixed the value of  $\delta$  determined for sub-MEG-threshold excitation,

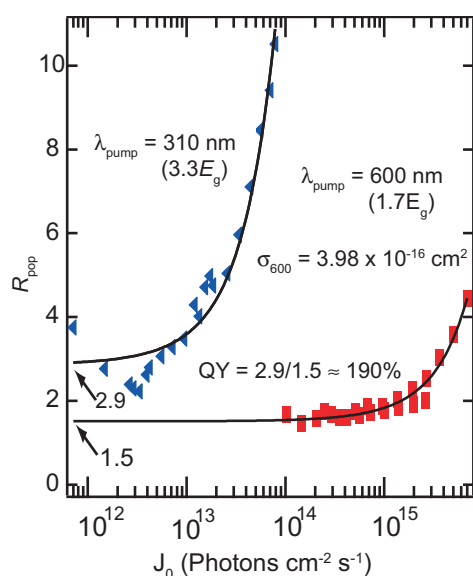


**Figure 12** (online color at: [www.lpr-journal.org](http://www.lpr-journal.org)) Ratio ( $R_{\text{pop}}$ ) of the exciton populations at 3 and 1200 ps are plotted vs. the pump photon fluence for a sample of Si NC with average diameter of 9.5 nm. The  $y$ -intercept represents the low-intensity limit of the ratio of the initial exciton population to the population after multiexciton states have decayed to single-exciton states.

and vary the QY. We find for the 9.5 nm sample that while the  $y$ -axis intercept is 1.5 when exciting below  $2E_g$ , the intercept of 2.9 for the case of  $3.3E_g$  excitation indicates a QY of  $1.9 \pm 0.1$ , indicating very efficient MEG.

## 2.5. Aspects of MEG

The simple energy threshold for production of two excitons from a single photon is twice the effective bandgap. Reports for the MEG threshold vary considerably over the range of  $2.0E_g$  (e.g., InAs/CdSe/ZnSe) to  $2.85E_g$  (e.g., PbSe), with some variation in the reported threshold for the lead-salt NCs (between  $2.0E_g$  and  $3.0E_g$ , per Ellingson and Murphy [14, 15], and  $2.85E_g$  per Schaller [16]). A straightforward model for the expected threshold dependence on electron and hole effective masses has been proposed and discussed by Schaller et al. [67] as well as by Pijpers et al. [61]. For semiconductor absorption of a photon with energy in excess of the bandgap, the excess energy is partitioned between the photogenerated carriers in accord with the inverse of their effective masses. In the absence of significant influence from the NC's detailed level structure, the excess energy of the electron and hole would be related through  $\Delta E_e = (m_h/m_e)\Delta E_h$ . If indeed the MEG process depends on the excess energy of a single carrier rather than the exciton, then under the assumption that  $m_h \geq m_e$  the photon energy threshold for MEG would be reached when

$$h\nu_{\text{thresh}} = \left(2 + \frac{m_e}{m_h}\right) E_g \quad (8)$$

Under these simple assumptions, the MEG threshold for PbSe NCs would occur at  $h\nu_{\text{thresh}} = 3E_g$  since  $m_e \approx m_h$ ; for InAs NCs, where  $m_h/m_e \approx 19$ , the MEG onset would be predicted to occur at  $h\nu_{\text{thresh}} = 2.05E_g$ , in accord with results reported by Schaller et al. [68]. Detailed balance analyses of photovoltaic device efficiency in the presence of MEG have shown that, as expected, the threshold energy plays a critical role in the achievable conversion efficiency [9, 69]. Specifically, an ideal MEG-active device can achieve efficiency of  $\sim 42\%$  for an MEG threshold of  $2E_g$ , whereas an MEG threshold of  $3E_g$  reduces the ideally attainable efficiency to  $\sim 35\%$ , only slightly above the Shockley-Queisser limit of  $\sim 33\%$ . Further discussion of detailed experimental results for each NC type will be presented below.

Another critical concern for achievable device efficiency pertains to the slope efficiency of production of additional excitons above the threshold photon energy. Ideally, the absorber would follow the "staircase" curve (Fig. 13a solid line) such that *all* photons with  $h\nu > (N)E_g$  would produce  $N$  excitons convertible into  $N$  photocurrent electrons. Observations to date show MEG quantum yield slope efficiencies of  $\gtrsim 100\%/E_g$  for PbSe and CdSe NCs to  $\sim 35\%/E_g$  for InAs core-shell NCs [67, 68]. An optimal combination of NC bandgap, MEG threshold, and slope

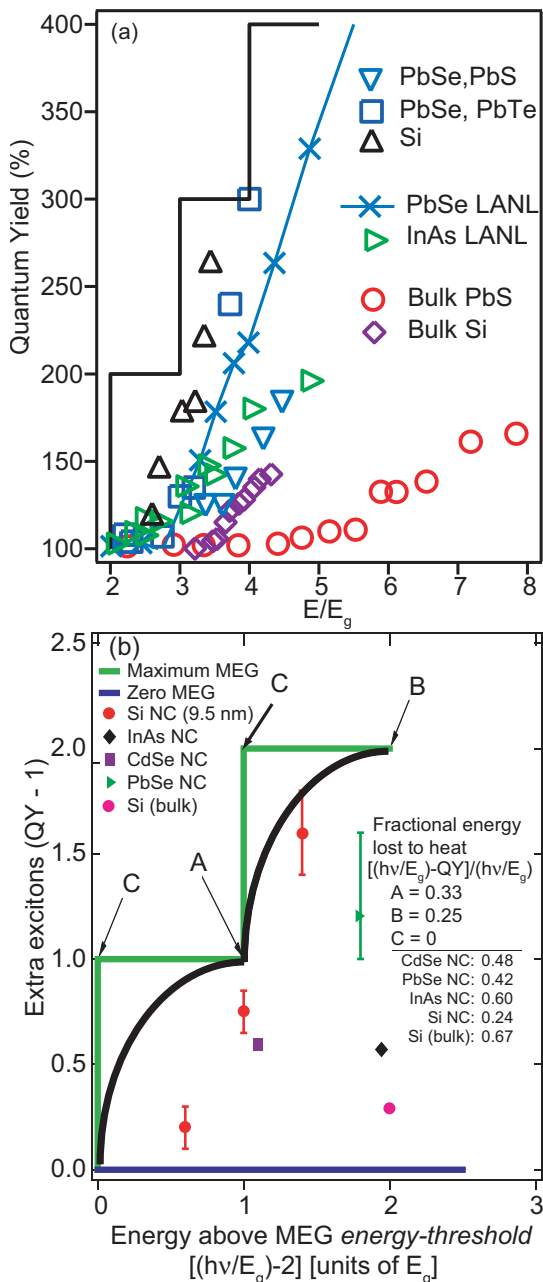


**Figure 13** (online color at: [www.lpr-journal.org](http://www.lpr-journal.org)) (a) MEG quantum yield values compiled for several reports on PbSe, InAs, and Si NCs, plotted with quantum yields from impact ionization data for bulk Si and bulk PbS. (b) The efficiency of the MEG process for selected data points based on spectroscopic measurements by various authors. Data are graphed as the production of extra excitons vs. the excess energy above the energy threshold ( $2E_g$ ) for MEG. The blue curve applies to the case for no MEG; the green curve shows the optimal Mmax staircase where photons of energy  $nE_g$  produce  $n$  excitons total; and the black curve depicts a reasonable scenario corresponding to the potential for enhanced device performance. The closer a data point lies to the black curve (or green curve), the lower the fractional energy lost to heat. The least fractional energy lost to heat for these data occurs for reported MEG QYs in Si NCs.

efficiency would be  $E_g \sim 0.9\text{--}1.1$  eV range would be  $2E_g$  and  $100\%/E_g$ . Fig. 13b shows how reported MEG values for selected excitation energies result in different amounts of average energy loss as heat.

### 3. Nanocrystalline semiconductors exhibiting multiple exciton generation

Efficient MEG has been reported for NCs of PbSe, PbS, CdSe, PbTe, InAs, and Si. We show in Fig. 13a the results for PbSe, InAs, and Si NCs compared to bulk II in PbS and Si. The evidence for efficient MEG consists of data from numerous time-resolved laser spectroscopy studies, of both colloiddally suspended nanocrystals as well as nanocrystal films, which show that photoexcitation at the level of a single photon per excited NC results in exciton population decay consistent with Auger recombination (see Sect. 2.4). The Auger recombination signature observed in these ultrafast time-resolved measurements indicates that, despite very low excitation fluence incapable of directly producing a significant multiexciton NC population, multiexciton states were produced through what has been *deduced* to be the MEG process. In addition to studies of NC solutions, one study of NC films showed that the MEG process remains efficient in layers consisting of either isolated or electronically coupled PbSe NCs [70]. Direct observation of the MEG process, which is understood to occur on a timescale of less than 100 fs, has not been reported. Although the effect appears to be general among a wide variety of NC types, there are variations in the reported values. This section will detail the reported results, and discuss issues associated with size-dependent efficiency, material-dependent MEG threshold, observations of MEG in core-shell NCs, and published reports of measurements showing much less efficient carrier multiplication in CdSe, CdTe, and InAs – reports which contradict other published results.

#### 3.1. Lead Salts – PbSe, PbS, PbTe, and PbSe-PbS core-shell NCs

The PbX NCs (PbSe, PbS, and PbTe) have many unique properties not found in other NC systems that make studying their size-dependent properties attractive from a basic fundamental aspect. The Bohr exciton sizes for PbSe, PbS, and PbTe are 46 nm, 20 nm, and  $\sim 80$  nm, respectively, while it is only  $\sim 6$  nm for CdSe [15, 71]. The result of large Bohr exciton sizes is a more dramatic variation in confinement energy with NC size. The large confinement energies seen for the PbX NCs follow from a combination of small effective mass and large high-frequency dielectric constant ( $\sim 23$  for PbSe). The first measurements showing generation of multiple excitons in NCs resulting from photoexcitation at the single photon per NC level were reported by Schaller and Klimov for PbSe in 2004 [13]. The narrow bandgap (bulk PbSe  $E_g = 0.28$  eV) makes PbSe

an attractive candidate for MEG studies, since even with relatively strong confinement of  $\sim 400$  meV for the NC sizes studied, the effective bandgap ( $\sim 0.8$  eV, or 1550 nm) falls in the near-infrared region enabling relatively straightforward multiple-bandgap excitation photon energies. The initial measurements, which were conducted for three different sizes, showed a consistent threshold photon energy for MEG of  $3E_g$  and a peak MEG efficiency of 2.2 excitons produced per absorbed photon (quantum yield, QY) at an energy of  $\sim 3.7E_g$ .

Subsequent measurements by Ellingson, Beard, and Nozik et al. reported results for PbS and PbSe NCs showing QYs as high as 3.0 for PbSe (excitation at  $\sim 4E_g$ ) and 2.8 for PbS (excitation at  $\sim 4.5E_g$ ) [14]. These measurements reported a very strong likelihood of MEG occurring between  $2E_g$  and  $3E_g$ , however the MEG efficiency below  $3E_g$  were low ( $QY < 1.1$ ) and the data did not permit a further narrowing of the threshold energy value. In addition, the results reported by Ellingson et al. demonstrated that measuring the exciton population by probing the photoinduced absorption associated with intraband transitions yielded QYs equivalent to those measured using the interband bleach approach introduced by Schaller. The  $3E_g$  onset initially claimed by Schaller and Klimov was later revised slightly to  $\sim 2.85E_g$  [72]. MEG measurements by Murphy and Beard et al. on  $\sim 5.4$  nm diameter PbTe NCs also showed MEG [15], with a threshold for strong MEG at  $\sim 3E_g$  QYs similar to those reported for PbSe and PbS [14]. Measurements conducted by Beard et al. (unpublished, in collaboration with Lifshitz) for PbSe/PbS core/shell NCs [73] show MEG QYs which fall within the range of the values for other lead salt NCs shown in Fig. 12. Results for the several PbSe and PbS samples studied by Nozik et al. and Klimov et al. reveal considerable variation in reported QY values, with some reported measurements yielding lower MEG efficiencies, e.g.,  $QY \approx 1.9$  at  $\sim 4.5 E_g$ . Possible sources of the variation will be discussed below. Schaller et al. studied MEG under very high bandgap multiple excitation, reporting  $QY = 7.0$  at  $h\nu/E_g = 7.8$  for a sample of PbSe NCs with an effective bandgap of 0.636 eV [16]. Such extremely high exciton density produced very fast decays due to strong exciton-exciton annihilation.

### 3.2. Cadmium selenide

Perhaps the most commonly studied colloidal NCs for investigation of optical properties and charge carrier processes is CdSe. The electronic structure [22] and carrier cooling dynamics [74] are both well-characterized, and the surface chemistry has also been studied extensively. Several multiexciton studies have been conducted for CdSe to study the nonradiative and radiative decay of multi- and single-excitons within NCs, as well as the photon energy dependence of formation of multiexciton states for single photon excitation. As indicated above, contradictory results exist in the literature regarding the efficiency with which

MEG occurs. The initial report from Schaller et al. indicated that TA measurements on two different CdSe NC samples ( $E_g = 2.0$  eV and  $E_g = 2.1$  eV) showed MEG with an onset of  $\sim 2.5E_g$  and a QY that increased linearly with photon energy up to  $QY = 1.65$  at  $3.1E_g$  [67]. The authors noted that the slope (112%) of increasing efficiency closely matched that measured by them for PbSe (114%).

A subsequent publication from Schaller detailed MEG results for colloidally-suspended CdSe NCs employing time-resolved photoluminescence (TRPL) via the time-correlated single photon counting (TCSPC) technique [59]. As compared with TA, TCSPC offers improved sensitivity and better signal quality at low excitation level; on the other hand, biexciton lifetimes below about 100 ps cannot be easily resolved due to reduced temporal resolution of TCSPC. The authors demonstrated a high degree of equivalence between the two measurements techniques, noting that the presence of fast trap dynamics in some CdSe samples complicates the analysis.

Two other TRPL techniques can in principle be employed to measure the exciton population dynamics for a photoexcited NC sample: streak camera, and time-resolved PL by upconversion (also known as sum-frequency generation, or optical gating). Nair and Bawendi recently published a report on CdSe and CdTe NC samples in which they used a streak camera with  $\sim 2$  ps time resolution to characterize the PL decay signatures associated with the single exciton and biexciton states [62]. The authors studied the time dependence of the emission spectrum for direct excitation levels ranging from the single exciton to multiexciton level. Analysis of the integrated spectra corresponding to biexciton and single exciton emission enabled the extraction of an estimated radiative rate for the biexciton state ( $k_{BX}^{\text{rad}}$ ). The analysis indicated that the biexciton radiative rate exceeded that of the single exciton ( $k_X^{\text{rad}}$ ) by a factor of three instead of the factor of two one would arrive at by simple exciton counting. The authors posited that these conclusions affect the analysis of MEG QYs reported by Schaller et al. who assumed that  $k_{BX}^{\text{rad}}/k_X^{\text{rad}} = 2$  [59]. More significantly, when Nair et al. compared the band edge decay dynamics for low-intensity photoexcitation at  $h\nu < 2E_g$  to the dynamics at photon energies up to  $3.1E_g$ , they found no evidence of significant MEG occurring in NCs of either CdSe, CdTe, or core/shell NCs consisting of CdSe/ZnS or CdSe/ZnCdS. Sample degradation under high photon energy illumination was cited as a concern, and a note was included that highly-concentrated samples were used under short excitation exposure and stirring; sample integrity was monitored via decay dynamics throughout data collection.

### 3.3. (Indium arsenide)cadmium selenide (core)shell

Synthesis of bare colloidal InAs NCs yields samples with apparently very good size dispersion based on excellent

size-dependent optical absorption spectra. However, PL quantum yields are typically relatively low due to nonradiative recombination proceeding on the  $\sim 1$  ns timescale. In another clear victory for the core-shell approach to surface control, InAs core NCs overcoated with a double shell consisting of CdSe followed by ZnSe exhibit dramatically improved PL QY as well as PL lifetimes of  $\sim 200$  ns [75]. Such long single exciton lifetimes conform to the ideal dynamics for observing fast sub-nanosecond signatures of multiexciton decay in TA or potentially TRPL experiments. The first report of MEG occurring in these InAs core-shell NCs found that at  $\sim 2.7E_g$  the QY reached  $\sim 1.6$ . The report cited three different optical techniques, including interband TA, time-resolved terahertz spectroscopy (based on low-energy hole transitions in the valence band), and a quasi-continuous wave excitation spectroscopy. The threshold for MEG to occur was reported as  $2.14E_g$ . In addition, it was found that pre-pumping the sample to create one or more excitons reduced the efficiency of MEG via subsequent high photon energy excitation, in accord with the 1S level degeneracy of InAs. This report was subsequently corrected [61] to apparently retract all aspects of the report concerning efficient MEG (all other aspects of the reported carrier dynamics remain valid). In their correction, the authors cited major concerns regarding the ability to correctly determine the absolute per-NC absorption cross section (which scales linearly with the sample's linear optical density) and the possibility of intensity inhomogeneities in the excitation beam. Mentioned by Pijpers et al. as a possible but less likely factor in disagreement between the original and follow-up measurements was the potential influence of sample preparation since the NC samples came from different batches.

Schaller et al. reported on MEG studies of InAs NCs in a publication that followed the original report from Pijpers et al. but preceded that paper's correction. Schaller used TA spectroscopy and found that relatively efficient MEG occurred, with  $QY \approx 2.0$  for excitation at  $\sim 5E_g$ . The threshold was reportedly near  $2E_g$ . Due caution was exercised in this report to ensure the sample integrity under photoexcitation: results of TA measurements were included that demonstrated the effect of sample stirring versus a static sample, and no degradation effects were observed. The differences in the reports by Schaller et al. and Pijpers et al. represent another important issue which remains to be resolved. The Schaller study used only one shell overcoat InAs-CdSe shell while the Pijpers study used an InAs-CdSe-ZnSe core-shell-shell structure.

Indeed, the variation in reported QY values, together with conflicting reports regarding whether or not, or at least the efficiency with which, MEG occurs in CdSe and InAs, represent critical issues to resolve. Questions regarding whether and how the NC surface might play a role in the MEG process remain pressing. Furthermore, the ability to demonstrate concurrence regarding measurement results conducted by a meaningful number of research groups will prove essential in narrowing uncertainties in MEG QYs for a variety of semiconductor NC types.

### 3.4. Silicon

Silicon NCs, while less prevalent than other colloiddally-synthesized NCs, promise substantial application due to both the element's abundance and the broad knowledge base that exists for Si. Beard et al. investigated carrier multiplication using ultrafast TA to study three different sizes of colloidal Si NCs suspended in a nonpolar solvent [65]. The authors found that MEG occurs with considerably higher efficiency in Si NCs as compared to bulk Si, showing a threshold in 9.5 nm diameter NCs (effective band gap  $E_g = 1.20$  eV) to be  $2.4 \pm 0.1E_g$ , and this same size NC showed an exciton QY of  $2.6 \pm 0.2$  excitons per absorbed photon at  $3.4E_g$ . The measurements were the first reported occurrence of MEG in an indirect-gap semiconductor. The authors also investigated larger NCs and found that even for relatively small confinement energy of  $\sim 80$  meV, high photon energies produced efficient MEG. These observations raised considerable interest owing to the prominence of Si in solar photovoltaic technology, silicon's abundance within the Earth's crust, and its relatively low intrinsic toxicity.

## 4. Theoretical descriptions of multiple exciton generation

Because of the different electronic structure, an increased surface to volume ratio and Coulomb interaction as well as increased carrier-carrier interactions, a theoretical description of MEG will differ from that of I.I. in bulk materials. As we have discussed, MEG does not require momentum conservation as in bulk materials, and thus the MEG onset should be lower. Furthermore, in bulk materials free-carriers are produced while in NCs excitons are produced, and for this reason we prefer to use "MEG" rather than "carrier multiplication". To date there are not enough experimental results to unambiguously distinguish among the different theories. In particular, the rate of MEG has not been measured; however, MEG must occur within  $\sim 1$  ps after photon absorption. Any theory must explain the following experimental observations; the different MEG onsets for the various materials, the high efficiency compared to bulk I.I., fast and efficient MEG compared to much slower yet still efficient AR, the slope of the QY as a function of  $E/E_g$ , and the contradictory results reported for CdSe and InAs NCs. The slope of MEG with excess energy is not strongly dependent on the electronic structure of the NCs; however, we caution that some of the insensitivity may stem from large size dispersions in the semiconductor NC samples. The MEG onset, however, is dependent on material type. Theories must also predict any size-dependence, to date, experiments have not shown a clear size-dependence, but for very large NCs the enhanced MEG over that of bulk materials must decrease. No theory has yet been attempted to explain MEG when the NCs are strongly coupled in some fashion to their environment, a necessary requirement for solar energy conversion, or when the NCs are in an applied

field that is high enough to induce charge separation. An important experimental challenge is to measure MEG at the single NC level, which should enable substantial insight into the mechanism and concomitant advancement of predictive theories.

In general there are three theories that have been proposed to explain efficient MEG in semiconductor NCs; (1) a coherent superposition of single and multiple exciton states [14, 55]; (2) excitation of a virtual multiexciton state that is strongly coupled to a real multiexciton state [72, 76] and (3) incoherent impact ionization, analogous to bulk impact ionization with proper modification of the electronic states [77, 78].

Shabaev, Efros and Nozik [55] along with coworkers [14] report that a highly excited exciton is not an eigenstate of the multi-electron Hamiltonian and that therefore the single electron approximation is no longer valid. Single exciton states with sufficient excess kinetic energy form a coherent superposition with charged multi-exciton states of the same energy. A density matrix formalism is employed to describe the time evolution of the coherent superposition. They report conditions where highly efficient MEG can occur due to the relative dephasing rates of the biexciton and single exciton states and is also proportional to the Coulomb coupling between single and biexciton states. They show that even when the coupling is weak, MEG can be efficient as long as the biexciton rate dephases faster than the single exciton rate. A calculation of the biexciton dephasing rate vs. single exciton rate concluded that the biexciton does dephase faster than the single exciton [79]. Experimental measurements of the biexciton dephasing rate are challenging and have not been reported. As long as the ratio of these rates remains size independent, MEG will be size independent. For strong coupling, coherent quantum beats should be observable in the band-edge bleaching experiments. However, while some evidence suggests that this is occurring, the band-edge bleaching experiments are obscured by poor temporal resolution, large size-distributions, and the carrier-induced Stark shift all of which will tend to wash out any evidence of quantum beats between the single and biexciton states [14].

Rupasov, Klimov [72] and coworkers [76] propose that biexciton states can be created by direct absorption of photons that promote a virtual biexciton state, created by the Coulomb interaction between two valence band electrons, to a real biexciton state. Since multiexcitons are created by the absorption of light there is no rate of biexciton formation. The authors calculate the QYs using a second order perturbation theory and make an analogy to virtual Raman transitions. They find that the carrier multiplication yield is proportional to the ratio of the biexciton to single exciton density of states and the ratio of the intraband to interband transition matrix elements. They find that efficient MEG may occur even in the case of weak Coulomb coupling, and their calculation is consistent with the observed QY rise and is ascribed mainly to a rapidly increasing density of biexciton states relative to single exciton states.

Several research groups have calculated carrier multiplication yields via impact ionization [77, 78], where highly excited single excitons can undergo scattering to relax toward the band edge and promote an additional valence band electron into the conduction band. In these calculations Fermi's golden rule is used to calculate the MEG rate in a 1<sup>st</sup> order perturbation approach. Franceschetti, An, and Zunger use an atomistic pseudopotential method to calculate the density of states for single excitons and biexcitons. The I.I. transition matrix element, which is the inverse of the Auger recombination matrix element, depends upon the density of final states, in this case the biexciton state. They predict that the threshold for MEG occurs near where the density of biexciton states becomes greater than that of single exciton states and find, in PbSe NCs, that this occurs at about 2.3  $E_g$  in rough agreement with the MEG onset reported by the NREL group [14]. In a related calculation, Allan and Delerue [78] use tight binding calculations to determine the density of states and find that MEG can be very fast because the density of biexciton states rapidly increases for increasing  $E/E_g$ . They conclude that efficient MEG in NCs is not due to an enhanced Coulomb coupling. The difference in the AR vs. MEG rates is simply associated with the difference in the DOS between biexcitons and single excitons. At high photon energies they suggest that another mechanism may be needed to explain the experimental results.

It may be that some degree of all these theories plays a role in efficient MEG and which mechanism is operable depends on the excess energy and NC size. More experimental data of QYs for different material systems, surface passivation and dielectric environments, as well as careful measurements of cooling dynamics in order to extract biexciton and single exciton dephasing rates are needed in order to further understand and control MEG. An important point to make is that no theory has shown that MEG is not enhanced in NCs.

## 5. Nanocrystal solar cell devices with the potential to utilize MEG

To this point, we have discussed MEG in NCs that are suspended in solution, electronically isolated from one another. For useful electro-optic applications involving NCs, the NCs must be coupled electronically to their environment in some fashion. There are many different approaches envisioned to adequately couple to the NCs [12, 80]. For solar energy applications that attempt to harness the MEG-created electron-hole pairs there are several requirements that any approach must satisfy; (1) The NCs must be the active component, (2) efficient transport of electrons and holes, or excitons, must occur over macroscopic distances, and (3) the coupling can not be so strong as to reduce the MEG efficiency yet must be strong enough to separate the electron-hole pairs either by undergoing charge transfer or diffusing one exciton to a nearby NC that does not have an exciton prior to non-radiative Auger recombination.

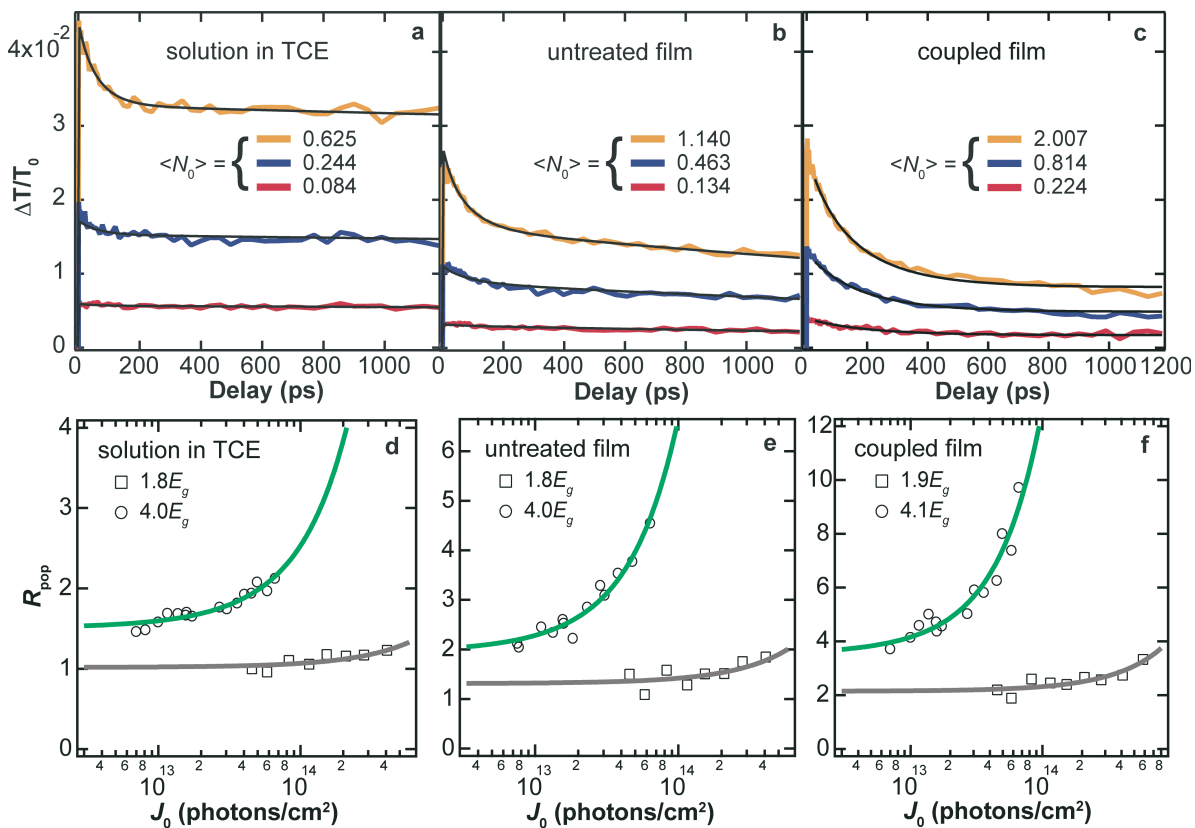


**Figure 14** (online color at: [www.lpr-journal.org](http://www.lpr-journal.org)) Comparison of exciton population decay dynamics measured for PbSe NCs in solution, and in weakly- and strongly-coupled in solid films, for photoexcitation below and above the energy threshold for the occurrence of MEG. (a–c) Carrier dynamics at sub-MEG threshold for increasing photon fluence  $\langle N_0 \rangle$  values are tabulated. (d–f)  $R_{pop}$  measurement for same samples in a–c for  $1.8E_g$  and  $4E_g$  excitation.

We have investigated an approach that incorporates 3-dimensional disordered arrays of NCs that exhibit strong inter-NC electronic coupling [70, 81–83]. The arrays may form the intrinsic region of a  $p-i-n$  configuration or the space-charge region of a Schottky-barrier solar cell. Exchanging the bulky capping ligands used in the NC synthesis with shorter molecules after film formation [84] can drastically increase the carrier mobility of NC films by reducing the inter-NC spacing while retaining relatively highly-passivated surfaces. A built-in electric field drives exciton dissociation, and the resultant charges then drift and/or diffuse to the electrodes for charge extraction. These quasi-free charges must avoid undergoing either surface trapping or recombination prior to extraction. Inter-NC coupling promotes exciton delocalization and thus favors charge extraction. As the strength of the coupling increases we expect that the MEG effect should decrease. To date we have not observed a decrease in MEG due to coupling, though all experimental data are in the weak coupling regime. A challenge for experimentalists is to measure the MEG efficiency as a function of inter-NC coupling strength, from isolated NCs to the bulk limit. It is important that excitonic features indicative of quantum confinement be preserved with any electronic coupling technique.

We compare the MEG efficiency in films that are treated with hydrazine to a film without chemical treatment and to a solution of NCs which remain electronically isolated. We observe three important effects that occur upon electronic coupling; (1) the absorption cross section per NC increases, (2) the biexciton lifetime increases, and (3) the MEG efficiency remains constant. Fig. 14a–c displays pump-probe band edge bleaching transients for the three different samples with  $1.8E_g$  excitation, below the MEG threshold. It is evident that both the biexciton lifetime as well as the single exciton lifetime change as a function of the chemical treatment. The biexciton lifetime increases from 67 to 116 ps between the solution and the films. All films that we have investigated to date show biexciton lifetimes significantly longer than those measured for isolated NCs in solution. The increase in biexciton lifetime can be understood by delocalization of the exciton wavefunction, as the biexciton lifetime in NCs is proportional to the volume. In the case of hydrazine treated films the increase in biexciton lifetime suggests that the exciton confinement radius increases by as much as 45% in the coupled film. The reduced confinement may be due to different surface polarization compared to NCs in solution or from wavefunction overlap with neighboring NCs. Fig. 14d–f displays  $R_{pop}$  measurements for the

three samples at  $1.8 E_g$  and  $\sim 4E_g$ , we find that MEG is essentially the same in the both films as it is in the isolated NCs [70]. Energy transfer from small NCs to large NCs may occur but should be relatively inefficient in these samples due to the small size dispersion and we do not see evidence for energy transfer on these timescales.

One challenge to producing efficient solar cells from NC films is the development of cracks. In the original film preparation procedure introduced by Talapin and Murray [83] a NC film is spin-cast or drop cast onto a substrate and the resulting film is then soaked in a suitable chemical treatment such as hydrazine to remove the bulky-capping ligands and potentially replace them with hydrazine. As a result of removing the ligands, the volume of the film can decrease by  $>40\%$  resulting in severe stresses and cracking. These stresses degrade device performance [63], even with a second round of NC deposition and a second round of treatment the stresses are not completely removed. Building the film with a layer-by-layer treatment, however, produces uniform, crack, and stress free films [82]. One potential drawback is any ordering of the NCs is lost when making the layer-by-layer film as each layer collapses due to the chemical treatment and the subsequent layer deposits NCs into the voids destroying any order. However, to date no effect due to disorder in the films has been observed.

Recently, large photocurrents have been reported [85]. These surprising results along with MEG bring new focus and attention to NC solar cells and solar energy conversion approaches based upon NCs. The device is of a very simple metal/NC/conductor (ITO) dielectric stack design. A Schottky barrier junction forms at the metal/NC interface and drives exciton dissociation and charge transport. There are challenges that need to be addressed before efficient MEG can be collected from this device. The Schottky contact is on the back junction making it difficult to collect carriers generated at the front of the device where higher-energy photons are strongly absorbed.

Other energy conversion approaches based on colloidal NCs include NC-sensitized nanocrystalline  $\text{TiO}_2$  [86–88] and NC-polymer blends [89,90]. In these types of devices, removal of the electrically insulating ligand shell surrounding each NC is vital for optimizing charge injection and can be accomplished with solution-based ligand exchange procedures. In one case where Jiang, Schaller and coworkers [89] built a device from a blend of PbSe NCs and P3HT, they observed a photoresponse from the PbSe NCs. Though they specifically looked for collected current arising from MEG, they did not find convincing evidence. They ascribe the lack of an enhanced photocurrent from MEG to poor charge transfer between the NCs and polymer and in fact their device efficiencies are rather low  $\sim 0.04\%$  with short circuit currents of  $\sim 0.2\text{mA}/\text{cm}^2$ . Improving the charge transfer may enable this device design to provide higher efficiencies and enable MEG carriers to be extracted prior to AR.

Approaches based on the NC-sensitized  $\text{TiO}_2$  may provide a means whereby the open circuit voltage could be improved over the Schottky solar cell. One potential draw-

back is that multiple-charges need to be extracted efficiently and this requires fast injection of electrons as well as holes to the electrolyte. Electrolytes that do not degrade the NCs are also necessary. Due to band alignment, charge injection from PbSe into  $\text{TiO}_2$  is not favorable and either a different NC material is needed or a different metal-oxide such as  $\text{SnO}_2$ .

## 6. Future directions

The reports of MEG in NCs have added to substantial previous work addressing unique and potentially important charge carrier processes such as carrier relaxation mechanisms and dynamics, and photoluminescence intermittency induced by Auger ionization. Interest in understanding the fundamentals of size-dependent charge carrier interactions has risen accordingly. Among the most pressing open research issues surrounding MEG pertains to clarifying the dependence of impact ionization (and MEG) and Auger recombination on confinement. Reports have been published which indicate that the Auger coefficient can be decreased in quantum wells lasers of  $\text{InAs}/\text{Ga}_{1-x}\text{In}_x\text{Sb}/\text{InAs}/\text{AlSb}$  [91]. And although several reports exist addressing the dependence of quantum yield on photon energy for several bulk semiconductors, most of the studies were conducted several decades ago and merit repeating. Since a substantial investigation of the size-dependence of carrier multiplication processes would provide essential knowledge for development of a “universal” size-spanning theoretical model, this stands as one of the major open questions of NC carrier processes.

Two obvious routes exist toward establishing the dimensionality and confinement dependence of MEG in NCs: effectively bottom-up, and top-down. Starting small, one could measure MEG for small spherical NCs, and reduce confinement effects either by increasing the NC size well beyond that of the Bohr exciton size, or one could increase just one dimension to modify the three-dimensionally confined nanostructures to two-dimensionally confined, as in nanorods (NRs). Such an effort presents evident challenges. For example, for the lead-salt NCs, growth of appropriate NRs would require lengths reaching to  $\sim 60\text{nm}$  (for PbS). In addition, large NCs show an increased propensity for aggregation, making stable suspensions less achievable. Lastly, the aforementioned spectroscopic techniques for observing MEG become more difficult in samples of larger NCs, due to the somewhat incongruous demands of large optical absorption cross section, low per-NC excitation level, and reasonably high signal level. Nonetheless, one can envision very interesting measurements based on, e.g., the influence of excitation polarization on MEG for NR samples. Starting with bulk crystals and moving to one-dimensional confinement represents another route to studying the size-dependence of MEG. In this case, challenges such as surface recombination and compatible high-energy barrier materials present unique challenges.

Another direction of interest for carrier multiplication in NCs includes the study of other candidate materials for photoconversion applications. Among the narrow-gap materials that may offer eventual application are Ge, SiGe (alloy-tunable bulk bandgap), InSb, CuInSe<sub>2</sub>, and amorphous semiconductors such as *a*-Si, *a*-Ge, or their alloys. While these studies in principle do not present insurmountable barriers, the ability to prepare high quality materials is necessary for practical studies. In general, carrier dynamics studies are best conducted on samples which show well-characterized optical properties, relatively long carrier lifetimes (e.g.,  $\geq 10$  ns), and ideally high emission QY (e.g.,  $> 10\%$ ). Based on the ability to synthesize Si NCs, synthesis of high-quality colloidal Ge NCs appears promising. Despite synthesis of high-quality III-V NCs, such as InP and InAs, InSb NCs have proven elusive.

In order to exploit MEG to the fullest, devices must be designed and achieved which enable the simultaneous features of efficient MEG and efficient photocurrent collection. In some cell designs the NCs are in the space-charge region of a Schottky junction. A built-in field of  $\sim 10$ – $30$  kV/cm<sup>2</sup> forms, driving exciton dissociation. Such a high field should modify the electro-optic properties of the NCs and may modulate the MEG effect. Understanding carrier dynamics under applied fields will be necessary to optimize power conversion efficiencies.

Another multiple exciton generation process occurs in molecular absorbers for which the singlet state lies at an energy equal to or slightly greater than twice the energy of the triplet state. Singlet fission (SF) results in the splitting of a singlet to form two triplet states, and in principle each triplet can contribute an electron to photocurrent. Singlet fission requires the ability to host two triplets – for example, a dimer, molecular crystal, or a polymeric molecule. The earliest examples of SF were reported for polyacenes such as tetracene and pentacene [92,93]. Active research in this area seeks to design molecular chromophores specifically for efficient SF [94,95].

## 7. Conclusions

Multiple exciton generation in semiconductor NCs provides a route to achieve efficient solar energy conversion at a potentially much lower cost. The NCs are synthesized in a low temperature wet chemistry fashion with potentially very low manufacturing cost. As-prepared NCs are suspended in solution and are then cast into thin films for device applications. One of the significant advantages to employing semiconductor NCs is that their properties may be tailored by size, shape, and surface manipulations. In particular the carrier dynamics are affected by all of these factors and are therefore under the control of synthetic chemists. Developing efficient solar cells that use NCs opens up a wide-range of new potential materials that can be explored to produce efficient solar energy conversion. The recent discovery of MEG in semiconductor NCs and its implications for enhanced energy conversion will serve to motivate researchers

to investigate and understand the various factors that govern carrier dynamics in semiconductor NCs.

We have reviewed the measurements to date of MEG in semiconductor NCs. Because of the importance of producing cheap renewable energy this field has received considerable attention and progress is rapid and growing. Most studies have relied on measuring MEG using ultrafast spectroscopic techniques. While the evidence for MEG is growing, two groups have reported results that are in contradiction to previously reported results. These differences must be reconciled. More work is needed to fully understand and control the carrier dynamics in semiconductor NCs. Understanding the specific interactions that result in efficient MEG and charge transfer as well as charge transport in nanoscale architectures will aid in the direct development of novel nanostructured materials for solar energy conversion, which may be in the form of electricity (photovoltaics) or fuels (photoelectrochemistry).

*Acknowledgements* The authors want to thank Arthur J. Nozik, Joseph M. Luther, Matt Law, Qing Song, Jeffrey Blackburn, Mark Hanna, Kelly Knutsen, Pingrong Yu, Justin Johnson, Kathrine Gerth, and James Murphy for valuable contributions to this work. We also acknowledge helpful conversations with Alexander Efros, and Andrew Shabaev. We thank Inger Jafari for help in manuscript preparation and Joseph Luther for help in preparing illustrations. Funding for this work was generously provided by the Chemical Sciences, Geosciences, and Biosciences Division, Office of Basic Energy Sciences, U. S. Department of Energy, under contract DE-AC36-99-GO10337 to the National Renewable Energy.



Matt Beard received his B. S. and M. S. degrees in Chemistry from Brigham Young University in 1997 and Ph. D. degree in Physical Chemistry from Yale University in 2002. He spent a year at the National Institute of Science and Technology before joining the group of Arthur Nozik at the National Renewable Energy Laboratory. His research activities include time-resolved THz spectroscopy for measuring the photoconductivity in nanoscale materials systems and the use of nanomaterials for efficient solar energy conversion



Randy Ellingson received his B. A. degree in Physics from Carleton College in Northfield, MN, and M. S. and Ph. D. degrees in 1990 and 1994 from Cornell University's department of Applied Physics. Since receiving the Ph. D. in 1994, Randy has conducted research on charge carrier dynamics in semiconductor for solar energy conversion, focusing on understanding how nanomaterials may ultimately lead to higher conversion efficiencies.

## References

- [1] M. A. Green, K. Emery, Y. Hishikawa, and W. Warta, *Prog. Photovolt., Res. Appl.* **15**, 425 (2007).
- [2] A. Slade and V. Garboushian, An improved high concentration solar cell and its implication for the mass production of high concentration PV systems, presented at the 21st European Photovoltaic Solar Energy Conference and Exhibition, Dresden, Germany, 2006 (unpublished).
- [3] W. Shockley and H. J. Queisser, *J. Appl. Phys.* **32**, 510 (1961).
- [4] R. R. King, D. C. Law, K. M. Edmondson, C. M. Fetzer, G. S. Kinsey, H. Yoon, R. A. Sherif, and N. H. Karam, *Appl. Phys. Lett.* **90**, 183516 (2007).
- [5] A. J. Nozik, *Annu. Rev. Phys. Chem.* **52**, 193 (2001).
- [6] P. T. Landsberg, H. Nussbaumer, and G. Willeke, *J. Appl. Phys.* **74**, 1451 (1993).
- [7] S. Kolodinski, J. H. Werner, T. Wittchen, and H. J. Queisser, *Appl. Phys. Lett.* **63**, 2405 (1993).
- [8] R. T. Ross and A. J. Nozik, *J. Appl. Phys.* **53**, 3813 (1982).
- [9] M. C. Hanna and A. J. Nozik, *J. Appl. Phys.* **100**, 074510/1 (2006).
- [10] M. Nirmal, B. O. Dabbousi, M. G. Bawendi, J. J. Macklin, J. K. Trautman, T. D. Harris, and L. E. Brus, *Nature (London)* **383**, 802 (1996).
- [11] A. L. Efros and M. Rosen, *Phys. Rev. Lett.* **78**, 1110 (1997).
- [12] A. J. Nozik, *Physica E* **14**, 115 (2002).
- [13] R. Schaller and V. Klimov, *Phys. Rev. Lett.* **92**, 186601 (2004).
- [14] R. J. Ellingson, M. C. Beard, J. C. Johnson, P. Yu, O. I. Mičić, A. J. Nozik, A. Shabaev, and A. L. Efros, *Nano Lett.* **5**, 865 (2005).
- [15] J. E. Murphy, M. C. Beard, A. G. Norman, S. P. Ahrenkiel, J. C. Johnson, P. Yu, O. I. Mičić, R. J. Ellingson, and A. J. Nozik, *J. Am. Chem. Soc.* **128**, 3241 (2006).
- [16] R. D. Schaller, M. Sykora, J. M. Pietryga, and V. I. Klimov, *Nano Lett.* **6**, 424 (2006).
- [17] U. Woggon, *Optical Properties of Semiconductor Quantum Dots* (Springer-Verlag, Berlin-Heidelberg, 1997).
- [18] A. P. Alivisatos, *J. Phys. Chem.* **100**, 13226 (1996).
- [19] A. L. Efros, in: *Semiconductor Nanocrystals*, Vol. 6, edited by A. L. Efros, D. J. Lockwood, and L. Tsybeskov (Kluwer Academic / Plenum Publishers, New York, 2003), p. 52.
- [20] A. L. Efros and A. L. Efros, *Sov. Phys.-Semicond.* **16**, 772 (1982).
- [21] L. E. Brus, *J. Chem. Phys.* **80**, 4403 (1984).
- [22] D. J. Norris and M. G. Bawendi, *Phys. Rev. B* **53**, 16338 (1996).
- [23] A. L. Efros, V. A. Kharchenko, and M. Rosen, *Solid State Commun.* **93**, 281 (1995).
- [24] P. Guyot-Sionnest, M. Shim, C. Matranga, and M. Hines, *Phys. Rev. B* **60**, R2181 (1999).
- [25] V. I. Klimov, A. A. Mikhailovsky, D. W. McBranch, C. A. Leatherdale, and M. G. Bawendi, *Phys. Rev. B* **61**, R13349 (2000).
- [26] J. L. Blackburn, R. J. Ellingson, O. I. Mičić, A. J. Nozik, *J. Phys. Chem. B* **107**, 102 (2003).
- [27] P. Guyot-Sionnest, B. Wehrenberg, and D. Yu, *J. Chem. Phys.* **123**, 074709 (2005).
- [28] A. R. Kortan, R. Hull, R. L. Opila, M. G. Bawendi, M. L. Steigerwald, P. J. Carroll, and L. E. Brus, *J. Am. Chem. Soc.* **112**, 1327 (1990).
- [29] M. A. Hines and P. Guyot-Sionnest, *J. Phys. Chem. B* **100**, 468 (1996).
- [30] V. I. Klimov, A. A. Mikhailovsky, D. W. McBranch, C. A. Leatherdale, M. G. Bawendi, *Science* **287**, 1011 (2000).
- [31] R. Koole, G. Allan, C. Delerue, A. Meijerink, D. Vanmaekelbergh, and A. J. Houtepen, *Small* **4**, 127 (2008).
- [32] I. Kang and F. W. Wise, *J. Opt. Soc. Am. B* **14**, 1632 (1997).
- [33] J. J. Peterson, L. B. Huang, C. Delerue, G. Allan, and T. D. Krauss, *Nano Lett.* **7**, 3827 (2007).
- [34] P. Liljeroth, P. A. Z. van Emmichoven, S. G. Hickey, H. Weller, B. Grandidier, G. Allan, and D. Vanmaekelbergh, *Phys. Rev. Lett.* **95** (2005).
- [35] S. V. Kilina, C. F. Craig, D. S. Kilin, and O. V. Prezhdo, *J. Phys. Chem. C* **111**, 4871 (2007).
- [36] V. I. Klimov, *J. Phys. Chem. B* **104**, 6112 (2000).
- [37] T. Elsaesser and J. Shah, *Phys. Rev. Lett.* **66**, 1757 (1991).
- [38] W. S. Pelouch, R. J. Ellingson, P. E. Powers, C. L. Tang, D. M. Szmyd, and A. J. Nozik, *Phys. Rev. B* **45**, 1450 (1992).
- [39] W. S. Pelouch, R. J. Ellingson, P. E. Powers, C. L. Tang, D. M. Szmyd, and A. J. Nozik, *Semicond. Sci. Technol.* **7**, B337 (1992).
- [40] H. K. Jung, K. Taniguchi, and C. Hamaguchi, *J. Appl. Phys.* **79**, 2473 (1996).
- [41] P. T. Landsberg, *Recombination in Semiconductors* (Cambridge University Press, Cambridge, 1991).
- [42] A. Smith and D. Dutton, *J. Opt. Soc. Am. B* **48**, 1007 (1958).
- [43] R. J. Hodgkinson, *Proc. Phys. Soc.* **82**, 1010 (1963).
- [44] O. Christensen, *J. Appl. Phys.* **47**, 690 (1976).
- [45] F. J. Wilkinson, A. J. D. Farmer, and J. Geist, *J. Appl. Phys.* **54**, 1172 (1983).
- [46] L. R. Canfield, R. E. Vest, R. Korde, H. Schmidtke, and R. Desor, *Metrologia* **35**, 329 (1998).
- [47] D. J. Erskine, A. C. Taylor, and C. L. Tang, *Appl. Phys. Lett.* **45**, 54 (1984).
- [48] A. J. Taylor, D. J. Erskine, and C. L. Tang, *J. Opt. Soc. Am. B* **2**, 663 (1985).
- [49] R. Korde and J. Geist, *Appl. Opt.* **26**, 5284 (1987).
- [50] W. Pötz, *Phys. Rev. B* **36**, 5016 (1987).
- [51] V. I. Klimov, D. W. McBranch, C. A. Leatherdale, and M. G. Bawendi, *Phys. Rev. B* **60**, 13740 (1999).
- [52] P. Yu, J. M. Nedeljkovic, P. A. Ahrenkiel, R. J. Ellingson, and A. J. Nozik, *Nano Lett.* **4**, 1089 (2004).
- [53] E. Hendry, M. Koeberg, F. Wang, H. Zhang, C. D. Donega, D. Vanmaekelbergh, and M. Bonn, *Phys. Rev. Lett.* **96** (2006).
- [54] J. M. Harbold, H. Du, T. D. Krauss, K. S. Cho, C. B. Murray, and F. W. Wise, *Phys. Rev. B* **72** (2005).
- [55] A. Shabaev, A. L. Efros, and A. J. Nozik, *Nano Lett.* **6**, 2856 (2006).
- [56] W. K. Metzger, M. W. Wanlass, R. J. Ellingson, R. K. Ahrenkiel, and J. J. Carapella, *Appl. Phys. Lett.* **79**, 3272 (2001).
- [57] D. I. Chepic, A. L. Efros, A. I. Ekimov, M. G. Ivanov, V. A. Kharchenko, I. A. Kudriavtsev, and T. V. Yazeva, *J. Lumin.* **47**, 113 (1990).
- [58] A. V. Barzykin and M. Tachiya, *J. Phys., Condens. Matter.* **19**, 065105 (2007).

- [59] R. D. Schaller, M. Sykora, S. Jeong, and V. I. Klimov, *J. Phys. Chem B* **110**, 25332 (2006).
- [60] D. Oron, M. Kazes, I. Shweky, and U. Banin, *Phys. Rev. B* **74**, 115333 (2006).
- [61] J. J. H. Pijpers, E. Hendry, M. T. W. Milder, R. Fanciulli, J. Savolainen, J. L. Herek, D. Vanmaekelbergh, S. Ruhman, D. Mocatta, D. Oron, A. Aharoni, U. Banin, and M. Bonn, *J. Phys. Chem. C* **112**, 4783 (2008).
- [62] G. Nair and M. G. Bawendi, *Phys. Rev. B* **76**, 081304 (2007).
- [63] M. Law, J. M. Luther, S. Song, B. K. Hughes, C. L. Perkins, and A. J. Nozik, *J. Am. Chem. Soc.* **130**, 5974 (2008).
- [64] M. Ben-Lulu, D. Mocatta, M. Bonn, U. Banin, and S. Ruhman, *Nano Lett.* **8**, 1207 (2008).
- [65] M. C. Beard, K. P. Knutsen, P. Yu, J. M. Luther, Q. Song, W. K. Metzger, R. J. Ellingson, and A. J. Nozik, *Nano Lett.* **7**, 2506 (2007).
- [66] D. Kovalev, J. Diener, H. Heckler, G. Polisski, N. Kunzner, and F. Koch, *Phys. Rev. B* **61**, 4485 (2000).
- [67] R. D. Schaller, M. A. Petruska, and V. I. Klimov, *Appl. Phys. Lett.* **87**, 253102 (2005).
- [68] R. D. Schaller, J. M. Pietryga, and V. I. Klimov, *Nano Lett.* **7**, 3469 (2007).
- [69] V. I. Klimov, *Appl. Phys. Lett.* **89**, 123118 (2006).
- [70] J. M. Luther, M. C. Beard, Q. Song, M. Law, R. J. Ellingson, and A. J. Nozik, *Nano Lett.* **7**, 1779 (2007).
- [71] F. W. Wise, *Acc. Chem. Res.* **33**, 773 (2000).
- [72] V. I. Rupasov and V. I. Klimov, *Phys. Rev. B, Condens. Matter Mater. Phys.* **76**, 125321 (2007).
- [73] E. Lifshitz, M. Brumer, A. Kigel, A. Sashchiuk, M. Bashouti, M. Sirota, E. Galun, Z. Burshtein, A. Q. LeQuang, I. Ledoux-Rak, and J. Zyss, *J. Phys. Chem. B* **110**, 25356 (2006).
- [74] V. I. Klimov and D. W. McBranch, *Phys. Rev. Lett.* **80**, 4028 (1998).
- [75] A. Aharoni, T. Mokari, I. Popov, and U. Banin, *J. Am. Chem. Soc.* **128**, 257 (2006).
- [76] R. D. Schaller, V. M. Agranovitch, and V. I. Klimov, *Nature Phys.* **1**, 189 (2005).
- [77] A. Franceschetti, J. M. An, and A. Zunger, *Nano Lett.* **6**, 2191 (2006).
- [78] G. Allan and C. Delerue, *Phys. Rev. B* **73**, 205423 (2006).
- [79] H. Kamisaka, S. V. Kilina, K. Yamashita, and O. V. Prezhdo, *Nano Lett.* **6**, 2295 (2006).
- [80] P. V. Kamat, *J. Phys. Chem. C* **111**, 2834 (2007).
- [81] J. E. Murphy, M. C. Beard, and A. J. Nozik, *J. Phys. Chem B* **110**, 25455 (2006).
- [82] J. M. Luther, M. Law, Q. Song, C. L. Perkins, M. C. Beard, and A. J. Nozik, *ACS Nano* **2**, 271 (2008).
- [83] D. V. Talapin and C. B. Murray, *Science* **310**, 86 (2005).
- [84] D. Yu, C. J. Wang, and P. Guyot-Sionnest, *Science* **300**, 1277 (2003).
- [85] J. P. Clifford, K. W. Johnston, L. Levina, and E. H. Sargent, *APL* **91**, 253117 (2007).
- [86] A. Zaban, O. I. Mičić, B. A. Gregg, and A. J. Nozik, *Langmuir* **14**, 3153 (1998).
- [87] C. H. Chang and Y. L. Lee, *Appl. Phys. Lett.* **91** (2007).
- [88] R. Vogel, P. Hoyer, and H. Weller, *J. Phys. Chem. C* **98**, 3183 (1994).
- [89] X. M. Jiang, R. D. Schaller, S. B. Lee, J. M. Pietryga, V. I. Klimov, and A. A. Zakhidov, *J. Mater. Res.* **22**, 2204 (2007).
- [90] S. A. McDonald, G. Konstantatos, S. G. Zhang, P. W. Cyr, E. J. D. Klem, L. Levina, and E. H. Sargent, *Nature Mater.* **4**, 138 (2005).
- [91] P. C. Findlay, J.-P. R. Wells, I. V. Bradley, J. G. Crowder, C. R. Pidgeon, B. N. Murdin, M. J. Yang, I. V. Vurgattman, and J. R. Meyer, *Phys. Rev. B* **62**, 10297 (2000).
- [92] S. J. Singh, W. J., W. Siebrand, B. P. Stoicheff, and W. G. Schneider, *J. Chem. Phys.* **42**, 330 (1965).
- [93] C. E. Swenberg and W. T. Stacy, *Chem. Phys. Lett.* **2**, 237 (1968).
- [94] I. Paci, J. C. Johnson, X. D. Chen, G. Rana, D. Popovic, D. E. David, A. J. Nozik, M. A. Ratner, and J. Michl, *J. Am. Chem. Soc.* **128**, 16546 (2006).
- [95] A. M. Muller, Y. S. Avlasevich, W. W. Schoeller, K. Mullen, and C. J. Bardeen, *J. Am. Chem. Soc.* **129**, 14240 (2007).
- [96] G. W. Charache, P. F. Baldasaro, L. R. Danielson, D. M. Depoy, M. J. Freeman, C. A. Wang, H. K. Choi, D. Z. Garbuzov, R. U. Martinelli, V. Khalfin, S. Saroop, J. M. Borrego, and R. J. Gutmann, *J. Appl. Phys.* **85**, 2247 (1999).
- [97] <http://www.ioffe.rssi.ru/SVA/NSM/Semicond/>.
- [98] P. C. Findlay, C. R. Pidgeon, R. Kotitschke, A. Hollingworth, B. N. Murdin, C. J. G. M. Langerak, A. F. G. van der Meer, C. M. Ciesla, J. Oswald, A. Homer, G. Springholz, and G. Bauer, *Phys. Rev. B* **58**, 12908 (1998).
- [99] R. Klann, T. Höfer, R. Buhleier, T. Elsaesser, and J. W. Tomm, *J. Appl. Phys.* **77**, 277 (1995).